Geophys. J. Int. (2006) **166,** 878–906 doi: 10.1111/j.1365-246X.2006.02991.x

Crustal structure of the central Nova Scotia margin off Eastern Canada

Yue Wu,[1] Keith E. Louden,[2] Thomas Funck,[3] H. Ruth Jackson[4] and Sonya A. Dehler[4]

[1]*Department of Earth Sciences, Dalhousie University, Halifax, Nova Scotia,* B3H 3J5, *Canada. E-mail: wuyue@phys.ocean.dal.ca*
[2]*Department of Oceanography, Dalhousie University, Halifax, Nova Scotia,* B3H 4J1, *Canada*
[3]*Department of Geophysics, Geological Survey of Denmark and Greenland (GEUS), Øster Voldgade* 10, DK-1350 *Copenhagen K, Denmark*
[4]*Geological Survey of Canada (Atlantic), Bedford Institute of Oceanography,* PO Box 1006, *Dartmouth, Nova Scotia,* B2Y 4A2, *Canada*

Accepted 2006 March 6. Received 2006 March 3; in original form 2005 April 5

SUMMARY

The central Nova Scotia margin off Eastern Canada is located at a transition from a volcanic margin in the south to a non-volcanic margin in the north. In order to study this transition, a wide-angle refraction seismic line with dense airgun shots was acquired across the central Nova Scotia margin. The 500-km-long transect is coincident with previous deep reflection profiles across the Lahave Platform and extending into the Sohm Abyssal Plain. A *P*-wave velocity model was developed from forward and inverse modelling of the wide-angle data from 21 ocean bottom seismometers and coincident normal-incidence reflection profiles. The velocity model shows that the continental crust is divided into three layers with velocities of 5.5–6.9 km s^{-1}. The maximum thickness is 36 km. A minor amount (∼5 km) of thinning occurs beneath the outer shelf, while the major thinning to a thickness of 8 km occurs over the slope region. The seaward limit of the continental crust consists of 5-km-thick highly faulted basement. There is no evidence for magmatic underplating beneath the continental crust. On the contrary, a 4-km-thick layer of partially serpentinized mantle (7.6–7.95 km s^{-1}) begins beneath the highly faulted continental crust, and extends ∼200 km seawards, forming the lower part of the ocean-continent transition zone. The upper part of the transition zone consists of the highly faulted continental crust and 4- to 5-km-thick initial oceanic crust. The continent–ocean boundary is moved ∼50 km farther seawards compared to an earlier interpretation based only on reflection seismic data. The oceanic crust in the transition zone consists of layer 2 and a high-velocity lower crustal layer. Layer 2 is 1–3 km thick with velocities of 5.6–6.0 km s^{-1}. The high-velocity lower crustal layer is 1–2 km thick with velocities of 7.25–7.4 km s^{-1}, suggesting a composite layer of serpentinized peridotite and gabbroic layer 3. Oceanic crust with normal thickness of 5–7 km and more typical layer 3 with velocities of 6.95–7.3 km s^{-1} is observed at the seaward end of the profile.

Key words: continental margins, crustal structure, Nova Scotia margin, refraction seismology.

1 INTRODUCTION

Rifted continental margins typically are classified into two major categories, volcanic and non-volcanic. Volcanic margins are characterized by seaward-dipping reflections (SDR) in the basement and thick underplated igneous rocks in the lower part of the thinned continental crust and initial oceanic crust, such as the US East Coast margins (Holbrook & Kelemen 1993; Talwani & Abreu 2000). Non-volcanic margins, on the other hand, are characterized by limited melt generation, which may be a result of slow extensional rates and cooling of the asthenospheric mantle during the long period of continental extension prior to break-up (Bown & White 1995). In this case, an ocean-continent transition (OCT) zone consists of either thin oceanic crust or exposed and serpentinized mantle (Louden & Chian 1999). Such serpentinized mantle rocks have been evidenced by drilling on the Iberia-Galicia Bank (Sawyer *et al.* 1994).

The Nova Scotia margin (Fig. 1) is located at the transition from volcanic margins to the south, e.g. the southern Baltimore Canyon Trough (Talwani & Abreu 2000), to non-volcanic margins to the north, e.g. the Grand Banks and Newfoundland Basins (Reid 1994; Funck *et al.* 2003). At the southern margin of Nova Scotia near Georges Bank, a strong, linear magnetic anomaly (∼300 nT), referred to as the East Coast Magnetic Anomaly (ECMA), is well developed. Deep marine seismic reflection profiles show SDR sequences on lines 89-3, 4 (Keen & Potter 1995a) coincident with the high-amplitude ECMA. The ECMA progressively weakens

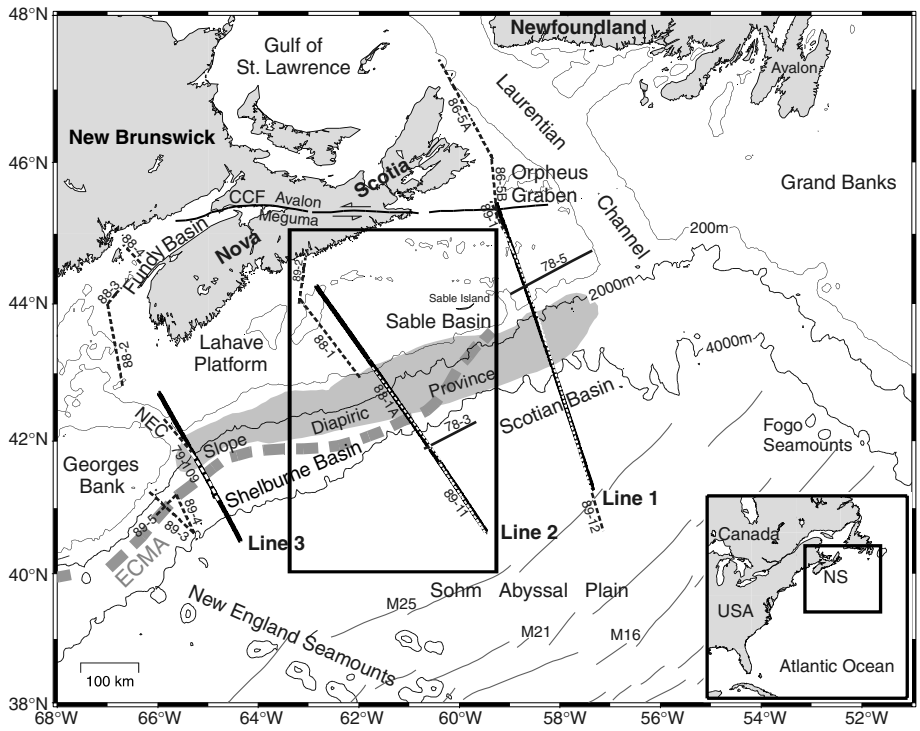

Figure 1. Location map of the Nova Scotia margin. The three refraction seismic lines of the SMART experiment are marked by bold solid lines. The rectangle outlines the area shown in Fig. 2. The inset shows the study region relative to eastern North America. The 200 m bathymetric contour is shown as a thin solid line; the 2000 and 4000 m contours are indicated by solid lines (National Geophysical Data Center 1988). The centre of the East Coast Magnetic Anomaly (ECMA) is marked by a dashed grey line (after Keen & Potter 1995b). Shaded area indicates the location of the Jurassic salt of the Slope Diapiric Province (after MacLean 1991). Magnetic lineations are shown as solid lines (Klitgord & Schouten 1986). Earlier seismic refraction lines 78-3, 5 (Keen & Cordsen 1981) are indicated by thin solid lines. Relevant MCS reflection lines in the study area are shown as dashed lines: lines 86-5A, 5B (Marillier *et al.* 1989); lines 88-1, 1A (Keen *et al.* 1991b), lines 88-2, 3, 4 (Keen *et al.* 1991a), lines 79-109, 89-11 and 89-12 (unpublished data by the German Federal Agency of Natural Resources and Geosciences, BGR), lines 89-3, 4, 5 (Keen & Potter 1995a); line 89-1 (Keen & Potter 1995b). The Cobequid Chedabucto fault (CCF) is shown as bold solid lines and arrows indicate the sense of displacement. Abbreviations are NS, Nova Scotia; NEC, Northeast Channel.

northwards and eventually disappears within the northern margin offshore Sable Island. The northern margin has been classified as a non-volcanic rifted margin without SDR sequence on line 89-1 (Keen & Potter 1995b). However, in the central segment of the Nova Scotia margin, the magnetic anomaly is still pronounced (∼200 nT), but there is no evidence for a SDR sequence on line 88-1A (Keen *et al.* 1991b) unless it is obscured by salt. The concurrence of magnetic and seismic signatures leads to an ambiguous character for the central margin segment.

In order to understand what controls the transition from volcanic margins to non-volcanic margins, the SMART (Scotian MARgin Transects) refraction seismic experiment (Fig. 1) was designed to image the along-strike variation in crustal structure at the transition from a volcanic to a non-volcanic style of rifting. Three wide-angle seismic refraction profiles (Lines 1–3) were acquired in 2001. Line 1 shows that the northern margin segment has an OCT zone of a highly serpentinized upper layer overlying a partially serpentinized lower layer, separating the highly thinned continental crust and oceanic crust by over ∼70 km of exposed mantle rocks (Funck *et al.* 2004). The results indicate that the northern Nova Scotia margin is non-volcanic. However, it is unknown if this is still valid for the central part of the margin.

This paper presents the results of Line 2 (Fig. 1). This line crosses the Lahave Platform and extends into the Sohm Abyssal Plain. Close to the coast, Line 2 runs parallel to a multichannel seismic (MCS) reflection line 88-1 and farther seawards it coincides with MCS line 88-1A (Keen *et al.* 1991b) and an unpublished line 89-11 acquired by the German Federal Agency of Geosciences and Natural Resources (BGR), forming a 500-km-long composite profile from the continental shelf to the deep ocean basin. The velocity model constrained by the wide-angle refraction data and the coincident MCS reflection profiles provides detailed information about crustal thinning and the ocean-continent transition. In this paper, we will show that the resulting velocity model also indicates a non-volcanic character across the central margin segment and therefore, that most of the Nova Scotia margin is primarily non-volcanic.

2 GEOLOGICAL SETTING

The Nova Scotia margin off Eastern Canada was formed within the Appalachian Orogen by the separation of Africa from North America during the Mesozoic break-up of Pangaea (Klitgord & Schouten 1986; Wade & MacLean 1990). Onshore, the basement of southern and central Nova Scotia consists of the Meguma terrane, intruded by granitoid rocks (Williams 1979; Keppie 1989). The Cobequid Chedabucto fault (CCF, Fig. 1) through the central Nova Scotia peninsula separates the Meguma terrane from the Avalon terrane to the north (Barr & Raeside 1989). Rifting of the Nova Scotia margin began in the Middle Triassic to Early Jurassic (230–175 Ma) (Welsink *et al.* 1989), followed by Jurassic seafloor spreading (Klitgord & Schouten 1986). The spreading rate for the initial

opening until magnetic anomaly M21 is ∼20 mm/year (Klitgord & Schouten 1986). Across the southern and central Nova Scotia margin, the Lahave Platform occupies the outer shelf and continental slope area, with the Shelburne Basin located on the continental slope. In contrast, across the northern margin segment, the Sable Basin with a thick wedge of both syn- and post-rift sediments is situated beneath the outer shelf. The oldest syn-rift deposits in the Sable Basin are non-marine Triassic redbeds, which are generally found between fault blocks (Wade & MacLean 1990). These are overlain by shallow marine sediments of Late Triassic–Early Jurassic age, including the extensive salt diapirs (Argo Formation) in the Slope Diapiric Province (Fig. 1; Welsink *et al.* 1989). The continent–ocean boundary is generally located seawards of the salt front (Keen *et al.* 1991b; Keen & Potter 1995a,b), except for the northern Nova Scotia margin where the salt front moved seawards (Sahabi *et al.* 2004; Shimeld 2004) during the upper Jurassic in response to Avalon uplift (Wade 1981).

3 SEISMIC EXPERIMENT

3.1 Data acquisition and processing

The wide-angle reflection/refraction seismic experiment was carried out onboard CCGS Hudson in 2001. Three lines were acquired cross the Nova Scotia margin (Fig. 1). The northern profile (Line 1) transects the Scotian Basin off Cape Breton Island. The middle profile (Line 2) extends from the Lahave Platform into the Sohm Abysmal Plain. The southern profile (Line 3) crosses the southwestern part of the margin near Georges Bank.

The seismic source was a tuned airgun array with a total volume of 104 L, consisting of 12 individual guns whose volumes range from 2.6–16.4 L. The airgun array was fired once a minute at an average ship's speed of 4.3 knots, resulting in an average shot spacing of 134 m. 21 ocean bottom seismometers (OBS) were deployed along Line 2 (Fig. 2). All the OBS were equipped with one hydrophone and three 4.5 Hz geophones. Instrument spacing varies from 32–40 km on the shelf (OBS 1–5) to 18–26 km farther seawards (OBS 6-21).

OBS and shot locations were determined by the Global Positioning System (GPS). Water depths along the profile were recorded by the ship's echosounder. A velocity-depth profile was derived from a conductivity, temperature and depth (CTD) measurement at 40° 30.86 ′N, 59° 41.42 ′W, near the southeastern end of Line 2. The CTD measurement was only conducted down to a depth of 2 km; downward extrapolation of the depth-velocity function was applied for greater depths.

Raw OBS data were downloaded and converted to SEGY format. Corrections for gun offset, gun delay and OBS clock drift were applied. The OBS positions at the seafloor are recalculated to fit the observed direct wave arrivals. All the data were debiased and filtered by a 5–10 Hz bandpass filter.

3.2 Methodology

A 2-D velocity model was developed using the program RAYINVR (Zelt & Smith 1992; Zelt & Forsyth 1994). Initially, a model was developed by forward modelling of observed traveltimes. Later, the forward model was refined by using the inversion algorithm of the program. The velocity model was primarily constrained by the OBS data. The bathymetry obtained by the ship's echosounder was used to define the seafloor geometry in the velocity model. The coincident MCS lines 88-1, 88-lA (Keen *et al.* 1991b) and 89-11 have been used to constrain the sedimentary layer boundaries and the detailed basement surface where the OBS data were not sufficient to determine the small-scale geometry. Sonic well-log data over the shelf and shallow slope were also used to constrain the sediment and uppermost basement velocities. A total of four wells (BASIN database, Geological Survey of Canada, Dartmouth, Nova Scotia, Canada) were used for comparison and calibration, with the maximum depth of 5.8 km at Acadia K-62 (Fig. 2).

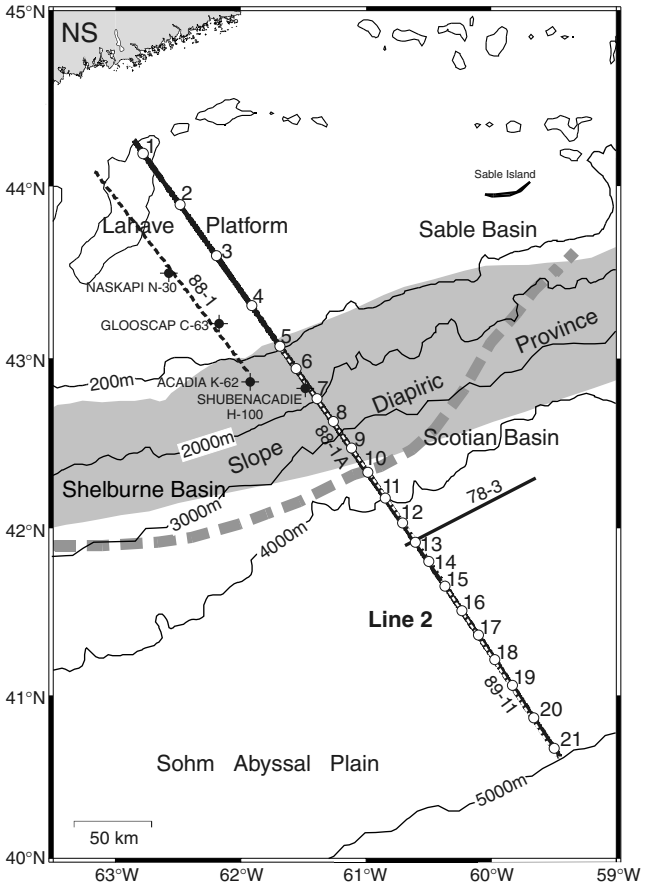

Figure 2. Location map for Line 2 (bold solid line). Positions of OBS are denoted as open circles and labelled with the instrument number. Filled circles overprinting on crosses mark the location of deep exploration wells in the vicinity of Line 2 (BASIN database, Geological Survey of Canada, Dartmouth, Nova Scotia, Canada). MCS lines 88-1, 1A (Keen *et al.* 1991b) and BGR line 89-11 (unpublished) are shown as dashed lines. Seismic refraction line 78-3 (Keen & Cordsen 1981) is shown as thin solid line. Bathymetric contours for 200 m, and 2000–5000 m with an interval of 1000 m are shown as solid lines. Other features as described in Fig. 1. NS, Nova Scotia.

The baseline for the 2-D velocity model was defined by the shooting line. The northwestern-most shot marks the start of the model and the southeastern-most shot defines the seaward end of the model. All the OBS locations and MCS sections (lines 88-1, 88-1A and 89-11) have been projected onto the baseline.

3.3 Data analysis

Record sections for OBS 1, 6, 11, 14 and 18 are shown in Figs 3–7, representative of the wide-angle data acquired along Line 2. Additional record sections are also included in Appendix A, including OBS 2, 5, 7, 8, 10, 15, 17 and 21. The horizontal distances in all these figures are relative to the starting point of the model.

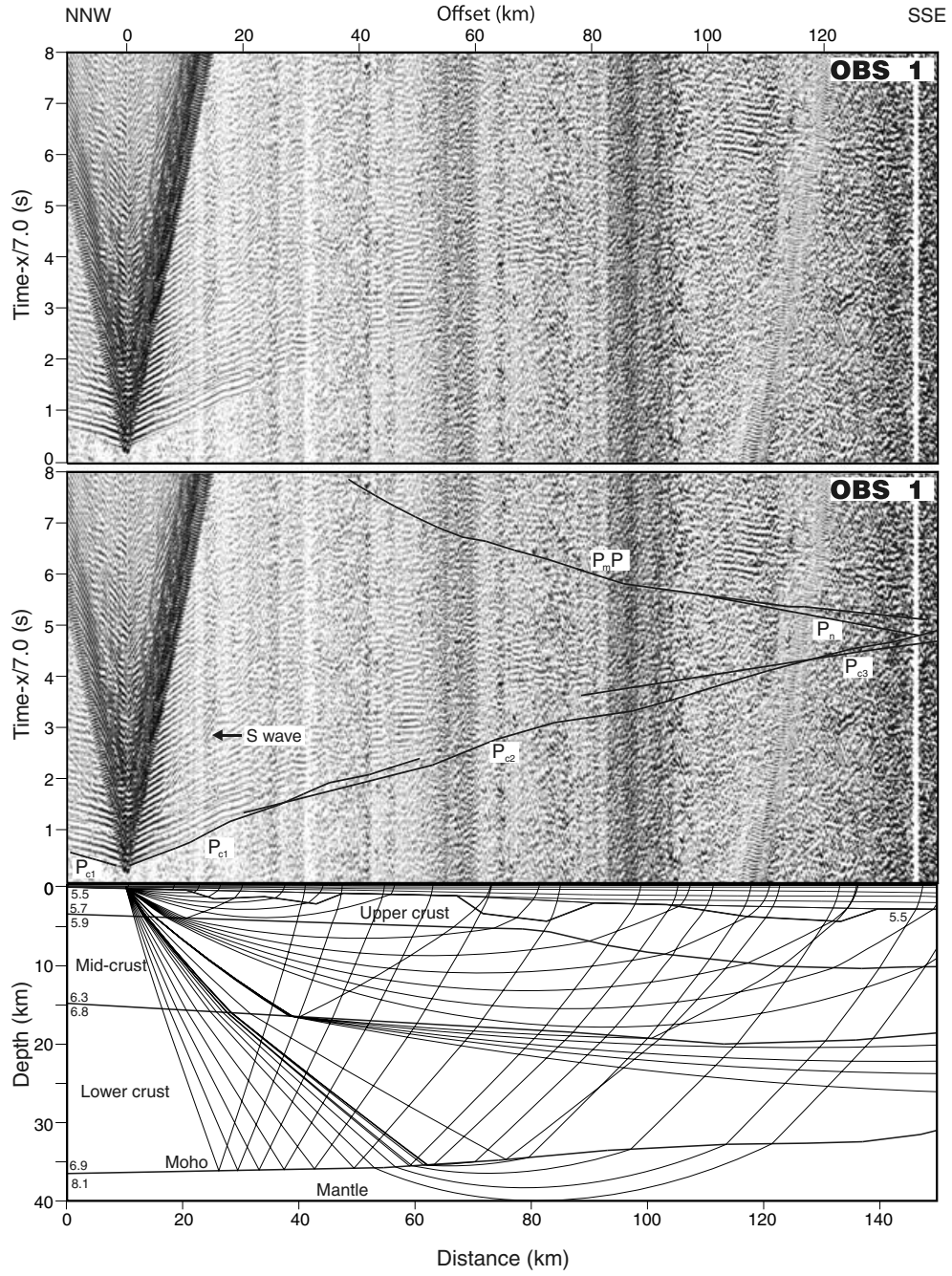

Figure 3. Record section (top), record section with calculated traveltimes (middle) and ray path diagram (bottom) for OBS 1 (hydrophone component). The horizontal scale of the record sections and the ray path diagram is distance along the velocity model (Fig. 8). Shot-receiver distance (offset) is also shown above the record section. The vertical scale in the record section is traveltime in seconds, displayed with a reduction velocity of 7.0 km s^{-1}. Numbers in the ray path diagram are *P*-wave velocity in km s^{-1}. Labels are defined in the text. The noise band in the data section at offset ∼120 km is noise from previous shots.

The phase nomenclature is based on the interpretation of individual layers in the velocity model. Refractions from the sedimentary layers S_1 through S_7 are named P_{s1} through P_{s7}. The reflections from the base of each of the sedimentary layers are denoted as $P_{s1}P$ through $P_{s7}P$, except for the reflection from the basement, which is labelled P_bP. P_{c1}, P_{c2} and P_{c3} are refractions from the upper, middle and lower continental crust, respectively; $P_{c1}P$ and $P_{c2}P$ are the mid-crustal reflections. Refraction and reflection from the oceanic layer 2 are labelled P_{L2} and $P_{L2}P$, respectively. The layer beneath layer 2 has anomalously high velocities. This layer is referred to as high-velocity lower crust (HVLC); its refraction and reflection are specifically named P_{HVLC} and $P_{\mathrm{HVLC}}P$, respectively. A layer underneath both continental and oceanic crust is later interpreted as partially serpentinized mantle (PSM); its refraction is labelled P_{n1}. Refraction from the 'normal' (i.e. unserpentinized) mantle is named P_n. The reflections from the top boundaries of the serpentinized and unserpentinized mantle are marked as $P_{m1}P$ and P_mP, respectively.

On the landward-most station OBS 1 (Fig. 3), P_{c1} is imaged, but P_{c2} and P_{c3} are weak and difficult to identify. Moho reflection (P_mP) and mantle refraction (P_n) are also observed, although the latter is less clear.

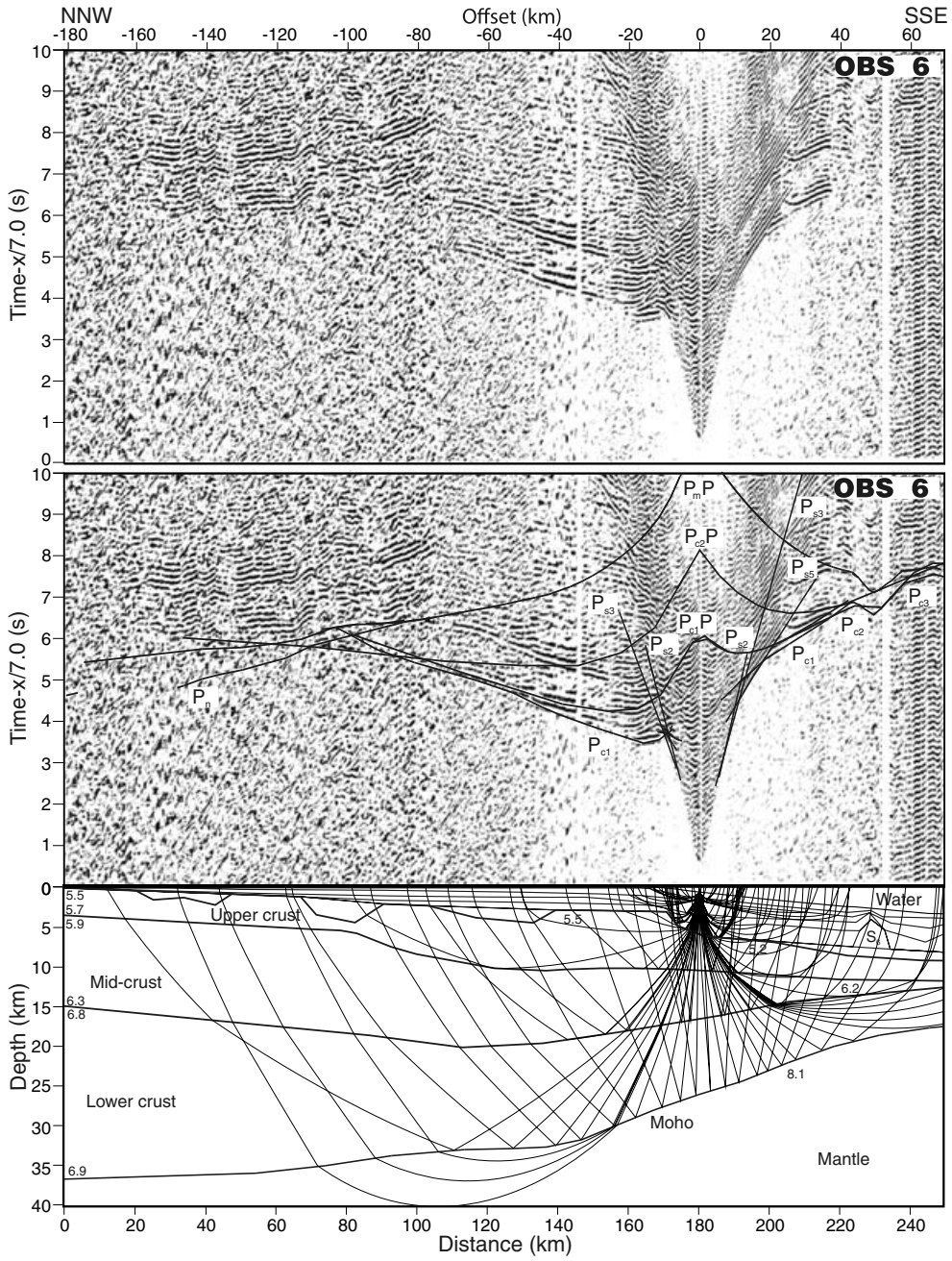

Figure 4. Record section (top), record section with calculated traveltimes (middle) and ray path diagram (bottom) for OBS 6 (hydrophone component). Features refer to Fig. 3.

OBS 6 (Fig. 4) is located ∼20 km seawards of the shelf edge. On this record section, P_{c1}, P_{c2} and the corresponding reflections P_{c1} P and P_{c2} P are observed. Moho reflection (P_mP) is imaged at far offsets. Mantle refraction (P_n) is less clear but identifiable at far offsets around −120 km.

OBS 11 is located at the seaward edge of the salt diapir structure (Fig. 5). Refractions from the salt units (P_{s6}) are observed. The P_{c1} phase is disturbed by the irregular geometry of the salt diapirs (S_6). The P_{c2} phase is not imaged on this section. The P_{c3} phase is imaged but on the SSE side it suddenly terminates at offset ∼50 km. Mantle refractions (P_n) are observed at far offsets.

OBS 14 (Fig. 6) is sited at the seaward edge of a series of faulted basement blocks (FB) imaged by coincident MCS data (Keen *et al.* 1991b). On the NNW side, P_{c1} appears as first arrivals between offsets −18 and −25 km with phase velocities of ∼5.0 km s^{-1}. In contrast, P_{L2} is imaged on the SSE side with phase velocities of 5.5–5.7 km s^{-1} (also see Fig. A6). In addition, P_{HVLC} appears on the SSE side with P-wave velocities (v_p) of 7.25 km s^{-1} but it is not observed on the NNW side. Furthermore, the P_{n1} phase is first observed as high-amplitude signals, indicating a relatively high-velocity gradient layer. The high-amplitude signals disappear at NNW side at offset −50 km, and they are not observed on stations further landwards, indicating that this layer terminates somewhere between distances 280–300 km. The reflection from its top boundary, which is termed P_{m1} P, is imaged on the SSE side. Phase P_n is observed at far offsets.

On OBS 18 (Fig. 7), phases P_{L2}, P_{HVLC}, P_{n1} and P_n are imaged on both sides as first or recognizable second arrivals. For P_{HVLC},

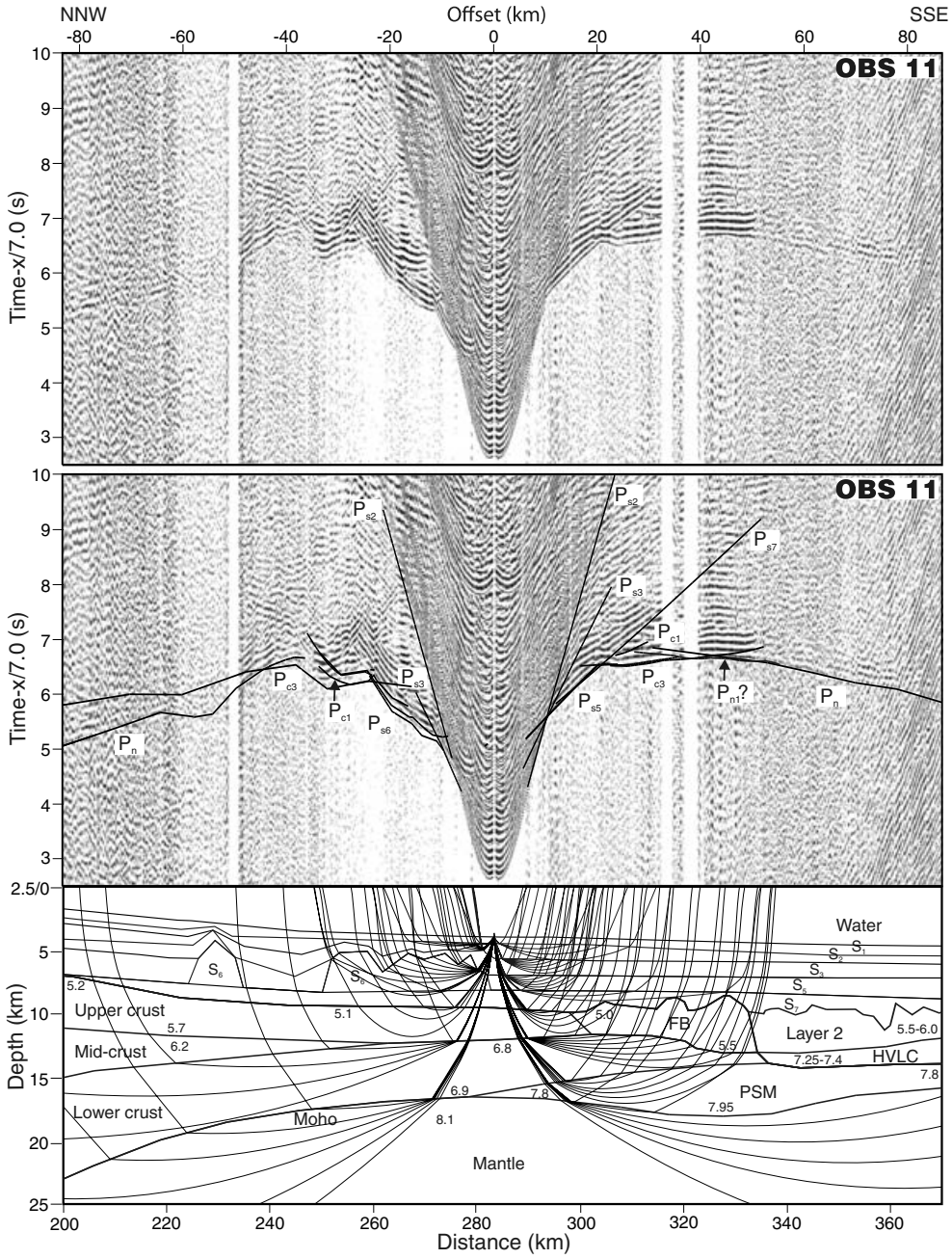

Figure 5. Record section (top), record section with calculated traveltimes (middle) and ray path diagram (bottom) for OBS 11 (vertical geophone component). Features refer to Fig. 3.

there is a change in velocity from 7.25–7.4 km s^{-1} in the NNW side to 6.95–7.3 km s^{-1} in the SSE side. The P_{n1} phase is observed on the SSE side at offset 60 km, but it no longer appears on the instruments farther seawards. This indicates that the layer producing the high-amplitude signals terminates seawards of OBS 18 at a distance of ∼480 km.

4 RESULTS

4.1 Velocity model

The *P*-wave velocity model for Line 2 is shown in Fig. 8. Sediments are divided into seven layers: S_1 to S_7. Velocities within the sediments vary from 1.7 to 4.6 km s^{-1}. Layers S_2, S_3, S_5 and S_7 are relatively flat layers over the deep sea basin with a total thickness of ∼6 km, but they thin and pinch out on the continental slope and shelf. The average velocity of 4.5 km s^{-1} for the salt diapirs (S_6) is constrained by the OBS data (Fig. 5) and is consistent with well-log results in Scotian Basin wells that penetrate the Argo Formation (Shimeld 2004). The boundary of the salt units is taken from coincident MCS line 88-1A (Keen *et al.* 1991b).

The continental crust has a maximum thickness of 36 km and is divided into upper, middle and lower crust with velocities of 5.5–5.7 km s^{-1}, 5.9–6.3 km s^{-1}, and 6.8–6.9 km s^{-1}, respectively. The continental crust thins gradually from the landward end of the line over a distance of 140 km. Most of the thinning occurs in the lower crust, while the total thickness of upper and middle crust is nearly constant. The upper crust may have included 1–3 km of carbonate

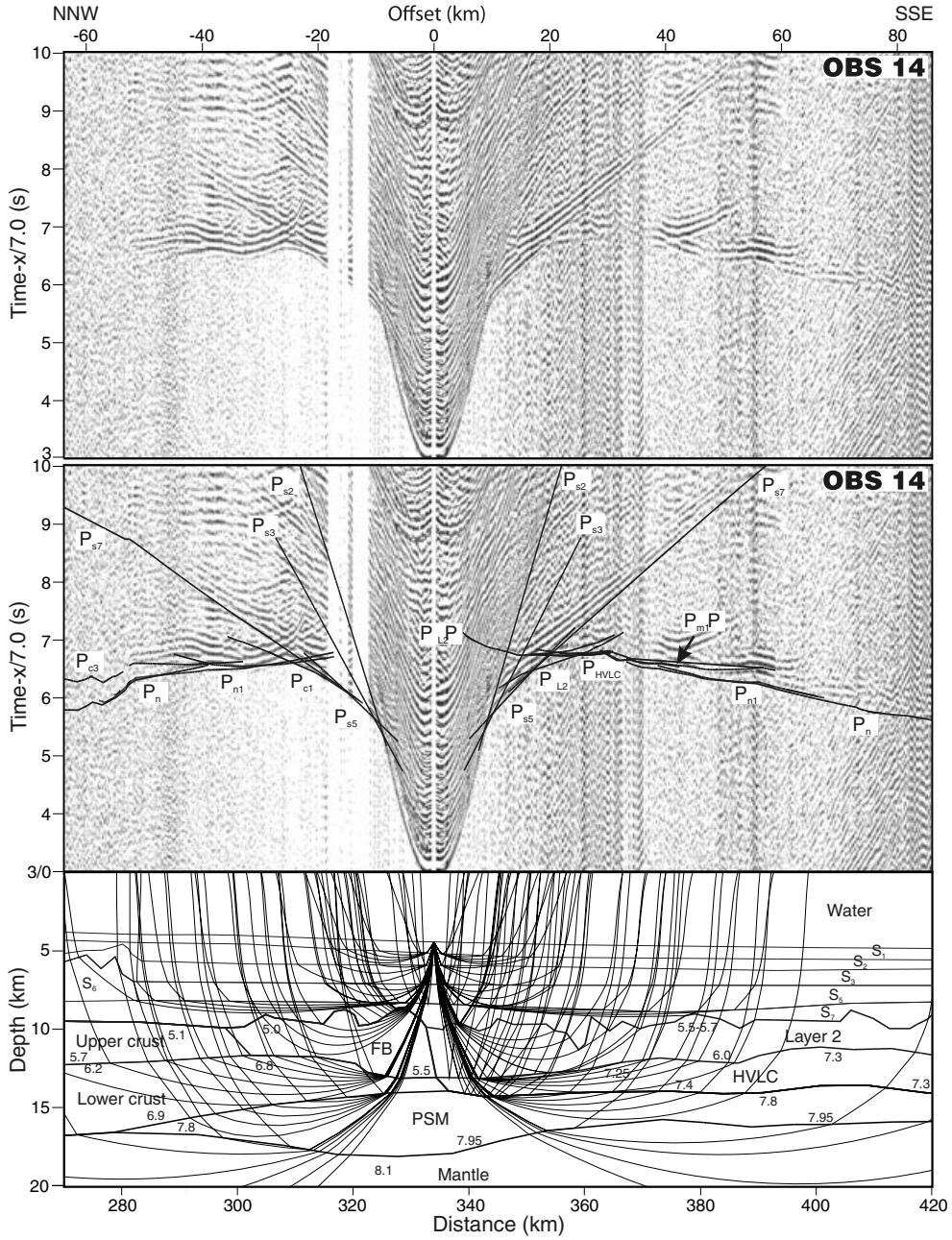

Figure 6. Record section (top), record section with calculated traveltimes (middle) and ray path diagram (bottom) for OBS 14 (vertical geophone component). Features refer to Fig. 3.

rocks at the shelf break, based on results from Acadia K-52. Farther seawards, the continental crust thins rapidly from ∼30 km thick at distance of ∼140 km to ∼8 km thick at distance of ∼240 km. Seawards of ∼220 km, the upper crust has a fairly constant thickness of ∼4 km and its v_p is reduced to 5.1 km s^{-1}. The FB between distance 290 and 330 km have v_p of 5.0–5.5 km s^{-1}. The middle crust disappears beneath the salt diapir. The lower crust terminates beneath the FB.

Seawards of the FB, oceanic layer 2 (L_2) is first encountered with v_p of 5.6–6.0 km s^{-1}. The variable basement topography is defined by the coincident MCS profiles 88-1A (Keen *et al.* 1991b) and 89-11. Below layer 2, a thin layer (∼1 km thick) is initially observed with v_p of 7.25–7.4 km s^{-1}. This layer is referred to as HVLC because the velocity is anomalously high, compared to that of a normal oceanic layer 3 (White *et al.* 1992). Its possible interpretations are discussed in Section 5.2.3. This layer thickens to ∼3.5 km at the seaward end of the model where its v_p decreases to 6.95–7.3 km s^{-1}, which is more typical of layer 3 (L_3, Fig. 8).

A layer with v_p of 7.6–7.95 km s^{-1} beneath highly thinned continental crust and oceanic crust extends from 280 to 480 km (Fig. 8). The maximum thickness of this layer is ∼4 km at the continent–ocean boundary (COB) with a velocity gradient of ∼0.1 s^{-1}. Farther seawards, this layer thins as the overlying basement thickens seawards. The nature of this layer is discussed in Section 5.2.4. Normal upper mantle appears at depths of 16.5–18 km with a velocity of 8.1 km s^{-1}.

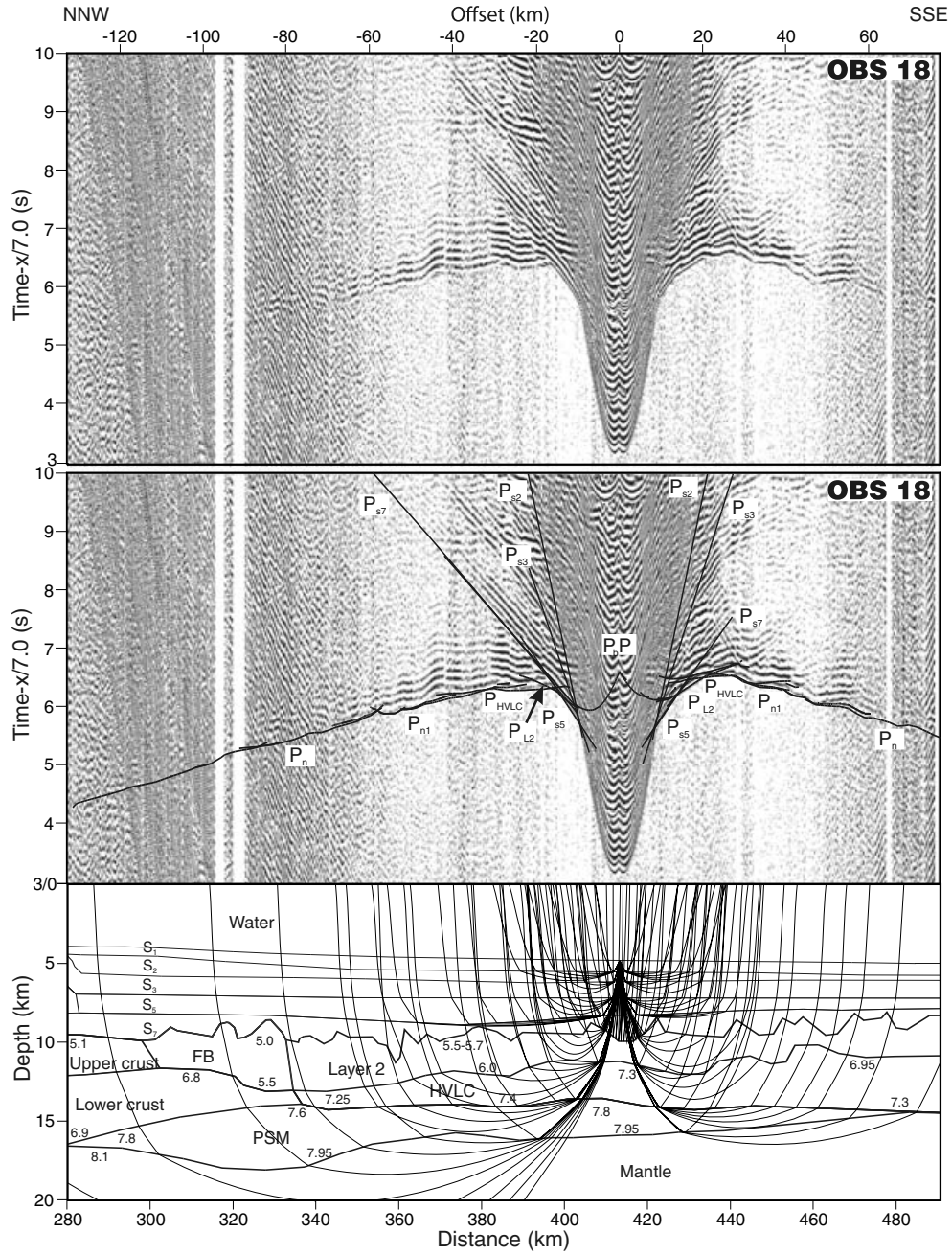

Figure 7. Record section (top), record section with calculated traveltimes (middle) and ray path diagram (bottom) for OBS 18 (hydrophone component). Features refer to Fig. 3.

4.2 Error analysis

The error analysis for individual phases is summarized in Table 1. The model is constrained with a total rms misfit of 82 ms between the calculated and picked traveltime arrivals. The normalized χ^2 of 1.015 is close to the optimum value 1.0 where the traveltimes are fit within the pick uncertainty. The pick uncertainties were assigned according to the signal-to-noise ratio and varied typically between 30 and 200 ms, with a few uncertainties up to 400 ms. The 'resolution' parameter of model is shown Fig. 9. A value of 1 indicates the model is perfectly parametrized, while a value of 0 suggests an uncontrolled model. Matrix diagonal values of >0.5 generally indicate reasonably well-constrained model parameters (Lutter & Nowack 1990). Although the method fits the traveltime, the slope of the phases is also well determined for phases that can be identified over a significant lateral extent. The sedimentary layers S_2–S_5 are well parametrized for both velocity and boundary nodes. The salt and uppermost sediment layer S_1 are poorly parametrized due to lack of ray coverage. Velocities for the upper continental crust, the serpentinized mantle and most of the normal mantle are well constrained. Some areas are less well constrained, such as the middle continental crust beneath the shelf edge and the landward part of the lower continental crust, where only limited refraction phases appear as clear arrivals. The velocities for the oceanic layer and the faulted blocks are also poorly parametrized due to the reduced ray coverage over this area caused by rough basement topography. The boundaries for upper continental crust and layer 2 and the HVLC layer are well parametrized while the middle and lower continental

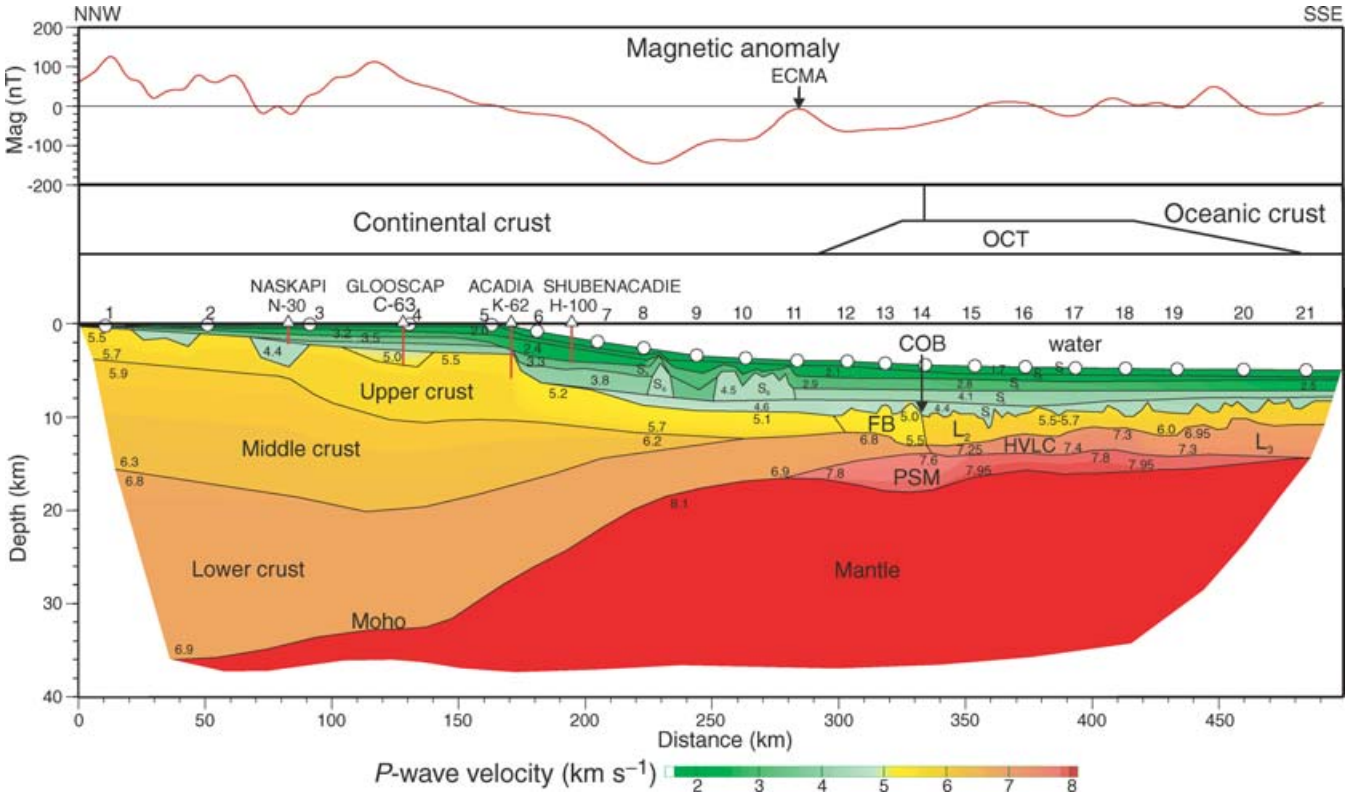

Figure 8. *P*-wave velocity model with colour scale (bottom) and coincident magnetic anomaly (top). A simplified interpretation of the crustal units is also illustrated (middle). Numbers within the velocity model are *P*-wave velocity in km s^{-1}. White circles mark the OBS locations with station numbers indicated above the velocity model. S_1 through S_7 are sedimentary layers 1 through 7. White triangles mark the location of deep exploration wells in the vicinity of Line 2 and the vertical red lines show their depths. The magnetic profile (top) is taken from Oakey & Dehler (2004). Abbreviations COB: continent–ocean boundary; ECMA: East Coast Magnetic Anomaly; FB: faulted blocks; OCT: ocean–continent-transition; L_2: layer 2; L_3: layer 3; HVLC: high-velocity lower crustal layer; PSM: partially serpentinized mantle.

Table 1. Number of observations (n), rms misfit between calculated and picked traveltimes (t_{rms}) and normalized χ^2 for individual phases.

Phase	n	t_{rms}, (ms)	χ^2
P_{s2}	663	44	1.291
P_{s3}	609	53	1.139
P_{s4}	206	64	0.476
P_{s5}	417	45	1.286
P_{s6}	37	174	2.212
P_{s7}	839	69	1.127
P_{c1}	744	72	0.839
P_{c2}	447	89	0.913
P_{c2} P	253	131	1.261
P_{c3}	379	72	0.940
P_{L2}	266	69	1.459
P_{L2} P	13	52	0.294
P_{L3}	343	53	0.743
P_{m1} P	36	146	2.207
P_{n1}	503	61	1.049
P_mP	830	134	0.763
P_n	1093	87	0.790
All phases	7678	82	1.015

crust and Moho are less well constrained. These results were only based on the refraction data. However, the velocity model boundaries are better defined because the major reflections (e.g. basement and Moho) within the coincident MCS sections were used to constrain the model (lower panel, Fig. 9), but were not included in the error analysis.

4.3 Gravity modelling

To verify the consistency of the velocity model with the observed gravity data, 2-D gravity modelling (algorithm of Talwani *et al.* 1959) was performed along Line 2. The observed gravity data are the satellite-derived free-air gravity anomaly (Sandwell & Smith 1997). The initial density model (Fig. 10b) was derived from conversion of *P*-wave velocity to density by using the empirical formula of Ludwig *et al.* (1970). To fit the regional gravity background, a density of 3.33 Mg m^{-3} was used for the sub-continental mantle up to a distance of 249 km, whereas a mantle density of 3.31 Mg m^{-3} was used farther seawards. This is consistent with the gravity model for Line 1 (Funck *et al.* 2004). The density of the salt units was reduced from 2.4 to 2.15 Mg m^{-3}, which is consistent with measurements from Scotian Basin wells (Shimeld 2004). With these adjustments, the calculated gravity fits the observed data with an overall misfit of ∼9 MGal (Fig. 10a). Some larger misfit (∼20 MGal) occurs over the shelf edge and slope. Due to the fact that a larger region of salt is located just to the south and north of Line 2 than imaged along this profile (MacLean 1991), the local misfit between distances 250–280 km is probably related to additional local salt mass deficiency. The lithostatic pressure over the slope region at the depth of 40 km is slightly elevated to 1130 MPa, compared to an average of 1125 MPa for this profile (Fig. 10c). To improve the fit over the shelf edge, an alternative model with the mantle 1.5 km shallower in this region (indicated by the dashed line in Fig. 10b) reduces the misfit of gravity anomaly but it causes misfits of the OBS data (see Figs 4, A3 and A4). Other models that reduce the depths of upper or middle

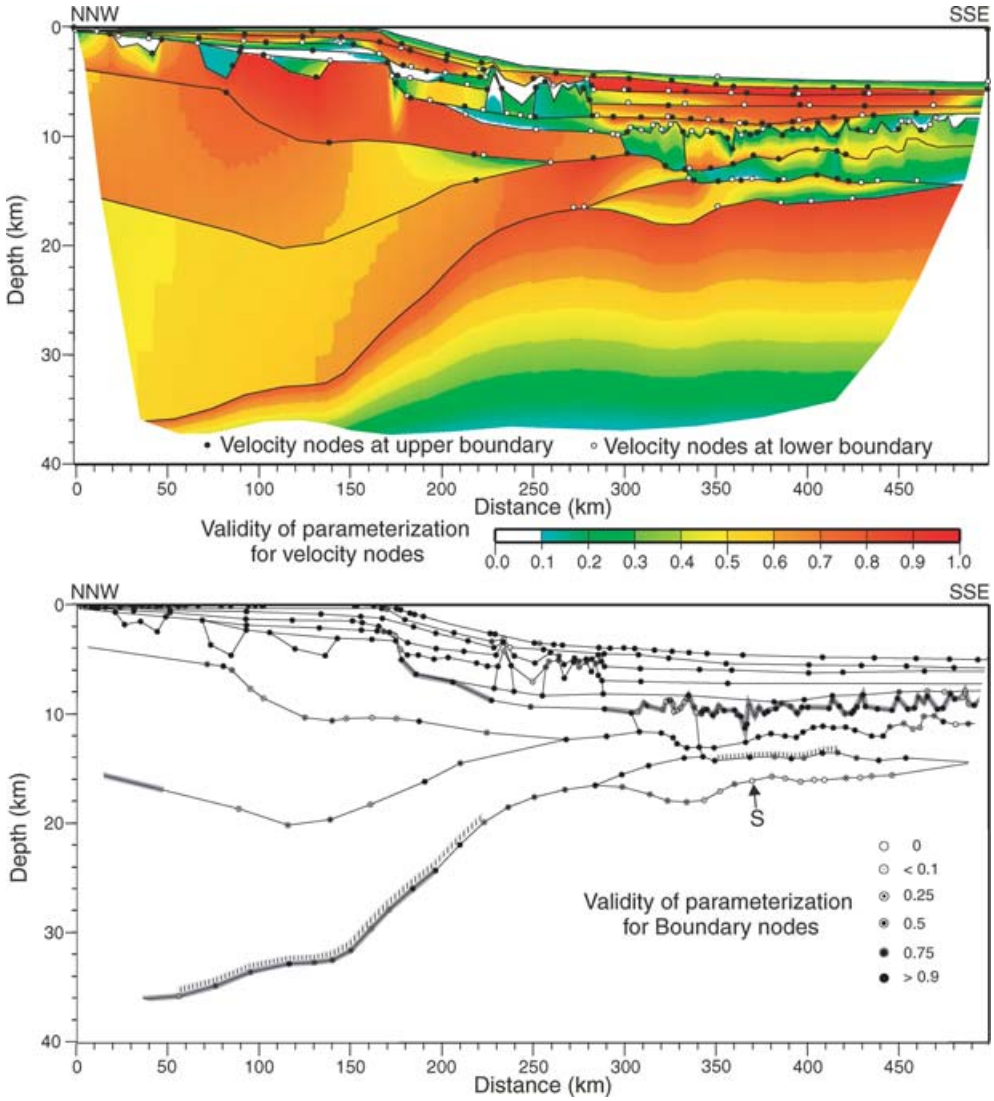

Figure 9. Resolution parameter of the *P*-wave velocities (upper) and boundaries (lower) for the model shown in Fig. 8. The validity of velocity nodes is represented by colours (upper). The velocity nodes for each layer are denoted as solid and open circles for upper and lower boundaries, respectively. To keep the velocity model as simple as possible, velocity nodes are placed only where the data indicate a velocity variation. The validity of the boundary nodes is represented as the percentage of fill in circles (bottom). Blanked area marks zones unconstrained by OBS data. Boundaries constrained by mantle reflections (P_mP or $P_{m1}P$) are indicated by hatched bars. Boundaries overprinted by thick shaded lines are also constrained by reflections in the coincident MCS sections. S marks the boundary from the serpentinized mantle to the unaltered mantle discussed in text.

crust also improve the gravity fit but they also decrease the fit of OBS data in a similar way. Therefore, these models are not preferred. The misfit at the landward end of the model was not investigated further because there are no seismic constraints landward of the line. Several granitic intrusions are known onshore (Benn *et al.* 1997) and in the near offshore (Loncarevic *et al.* 1994). Hence, some of the mass deficit at the landward end of the line might be related to lower density granites within the mid-crustal layer.

5 DISCUSSIONS

5.1 The rifted continental crust

The composite profile of MCS 88-1 and 88-1A converted from traveltime to depth using the velocity model shows that the velocity structure is consistent with the reflectivity (Fig. 11). Landwards of the shelf break, the upper and middle crust is less reflective except for a few northwest dipping reflections (e.g. W_1 and W_2) which flatten and terminate at the top of the lower crust. These reflections could represent pre-rift or post-rift normal faults within the Meguma terrane (Keen *et al.* 1991b). The velocity model indicates only minor crustal thinning coincident with the normal faults. This suggests that the northwest dipping fabric is more likely to be associated with the pre-rift structural grain although they may have been reactivated during rifting. While only a few reflections are observed in the middle crust, the lower crust is characterized by increased reflectivity, with the Moho following the base of a strong reflection band (M, Fig. 11). The initial crustal thinning seems to be mainly confined to the lower crust. The gently rising Moho reflection suggests that the crustal thinning begins at the northwestern end of the model, about 100 km farther landwards than previously predicted by subsidence analysis (Keen & Beaumont 1990). This will be discussed further in Section 5.3.2

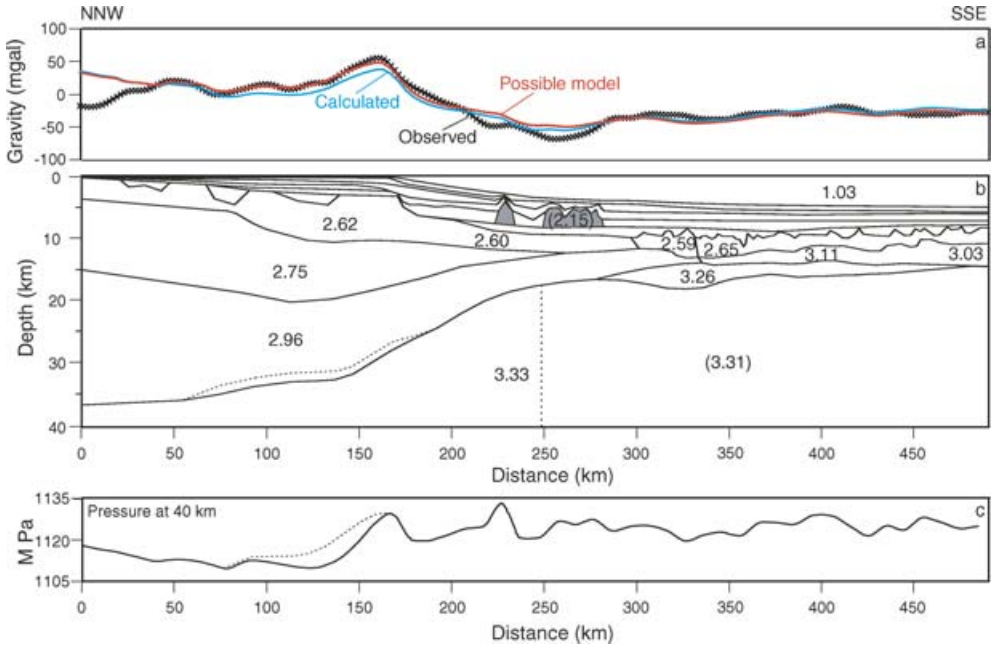

Figure 10. 2-D gravity modelling for Line 2. Top section (a) is the comparison of the observed and computed gravity anomalies shown by cross-hatched and green lines, respectively. The red line is the computed gravity anomaly from an alternative model shown by dashed line in (b). Middle section (b) is the density model directly converted from the *P*-wave velocity model (Fig. 8) by using the velocity–density relationship of Ludwig *et al.* (1970). To fit the observed gravity anomaly in (a), the density for the upper mantle beneath the oceanic crust and highly thinned continental crust is reduced from 3.33 to 3.31 Mg m^{-3} across the dotted line, and salt density is reduced from 2.4 to 2.15 Mg m^{-3}(indicated by the shaded region). Modifications are shown in parenthesis. Densities for sedimentary layers vary from 1.82 to 2.5 Mg m^{-3}. Densities in the model are given in Mg m^{-3}. To improve the fit at the shelf edge, an alternative model with the mantle 1.5 km shallower in this region (indicated by the dashed line) reduces the misfit of gravity anomaly (red line in panel a), but it decreases the fit of OBS data in this region (see Figs 4, A-3 and A-4). Bottom section (c) is the lithostatic pressure (solid line) at the base of the model at depth of 40 km, with a dashed line indicating the lithostatic pressure of the alternative model.

Seawards of the shelf break, the continental crust underwent an abrupt thinning beneath the hinge zone and southeast dipping reflections predominate (e.g. E_1, E_2). Unlike the pre-existing fabric beneath the shelf, the abrupt thinning of the continental crust is accommodated along the seaward-dipping faults, penetrating through the crustal layers and terminating at the Moho boundary. The Moho reflection is weak but still recognizable in this area, indicating that the continental crust extends at least to the landward edge of the salt. Beyond this point, the Moho reflections become ambiguous and the crustal thinning in the reflection section can not be traced further seawards. The reflectivity below the Moho boundary is obscure in this region, but the velocity model shows that there is no addition of a high-velocity (7.0–7.8 km s^{-1}) layer to the base of the abruptly thinned crust.

5.2 The ocean–continent transition (OCT) zone

The OCT zone in the velocity model extends from ∼280 to ∼480 km. Within the OCT, two anomalous velocity layers HVLC and PSM are overlain by continental crust in the NNW and oceanic crust in the SSE (Fig. 8). The various layers are discussed below.

5.2.1 Thinned continental crust

The two upper layers in the OCT zone up to a distance of ∼330 km are highly thinned continental crust (Fig. 8). This interpretation is based on the *P*-wave velocities derived from the OBS data and the characteristic basement reflectivity of the FB compared with basement structures elsewhere.

The OBS data indicate that the FB have a velocity of 5.0 km s^{-1}, which is almost the same as observed for the highly thinned continental crust beneath the slope (5.1 km s^{-1}). In contrast, it is ∼0.6 km s^{-1} lower than that of the upper basement layer seawards. The velocity for the FB is less well constrained because only a limited number of refraction first-arrivals are observed due to the rough basement topography across this region. However, this velocity is consistent with earlier observations of 4.62–5.27 km s^{-1} along refraction line 78-3 (Keen & Cordsen 1981) passing through the same region (Fig. 2). The velocities for the FB are more consistent with an interpretation of continental crust.

This interpretation is further supported by reflectivity of the FB (top, Fig. 12). Fanning reflectors against normal faults may indicate that layers are built up over a long period, while the pre-existing strata are being faulted and rotated, as for deposition in a subsiding half-graben. The half-grabens are bounded by rotated fault blocks and show similar geometry and reflectivity to those formed within rift-related depositional basins (e.g. Barents Sea; Prosser 1993). These features support the interpretation based on the OBS data and suggest that the onset of seafloor spreading is located seawards of the faulted basement structure (discussed in Section 5.2.2).

This revises previous interpretations based on MCS profiles 88-1A (Salisbury & Keen 1993; Keen & Potter 1995a,b). In their interpretations, the FB, based on the basement reflectivity and faulting, are interpreted as volcanic episodes at a slow-spreading ridge modified by tectonic rotation, and the COB lies at the seaward edge of the salt (Salisbury & Keen 1993). However, it is unlikely for slow spreading seafloor to retain long-lasting off-axis volcanism for

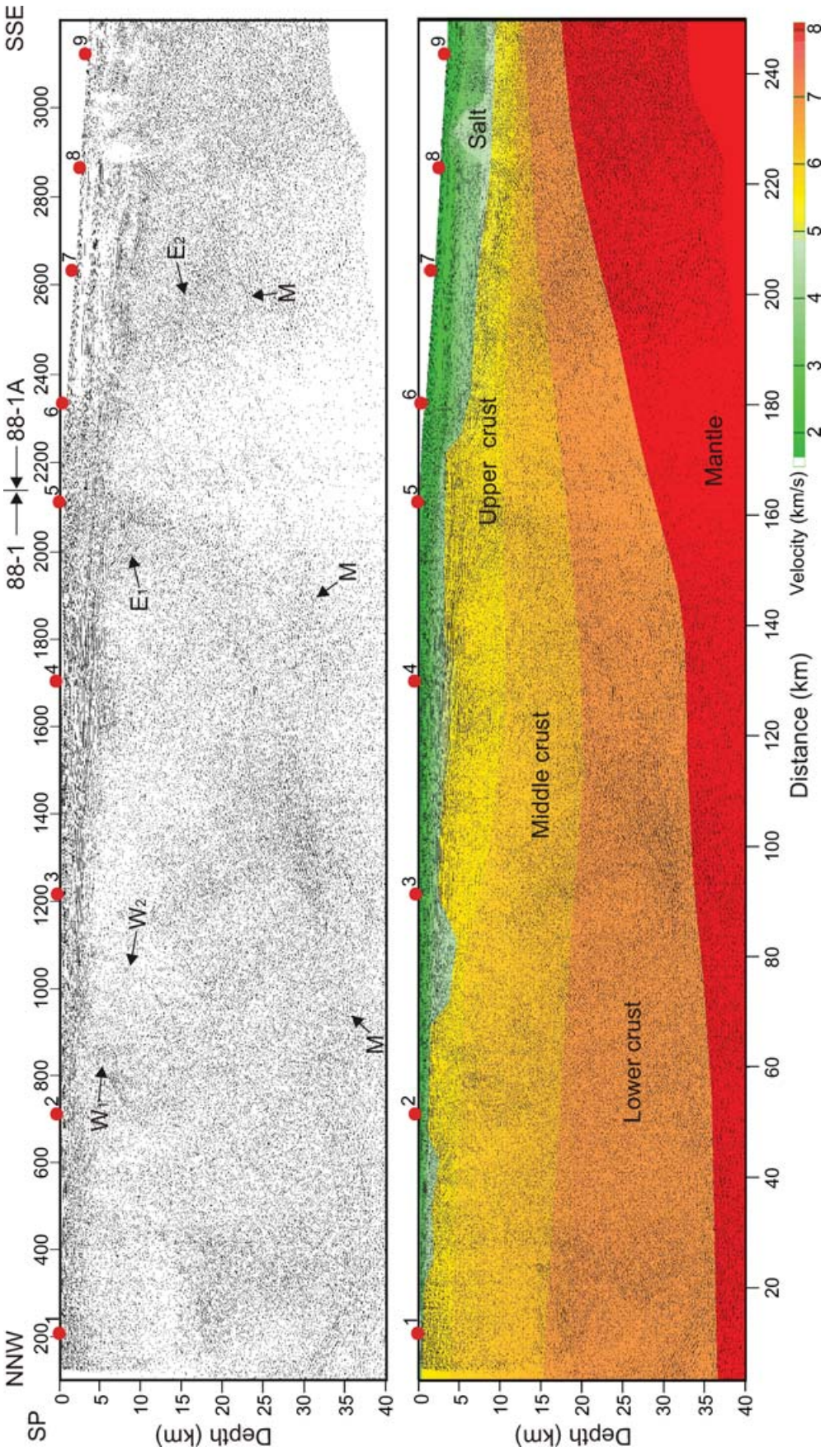

Figure 11. (Top) A composite MCS depth section of line 88-1 and part of line 88-1A (Keen *et al.* 1991b) converted from the two-way traveltime using the velocity model shown in Fig. 8. (Bottom) the same depth section shown together with the velocity model (colour scale). The horizontal scale is distance along the velocity model with the shot point (SP) number shown on top of the section. OBS positions are marked by red circles on the seafloor and labelled with numbers. Features marked by letters are W_1 and W_2, northwest dipping reflections; E_1 and E_2, southeast dipping reflections; M, Moho reflection. Vertical exaggeration: 1.5.

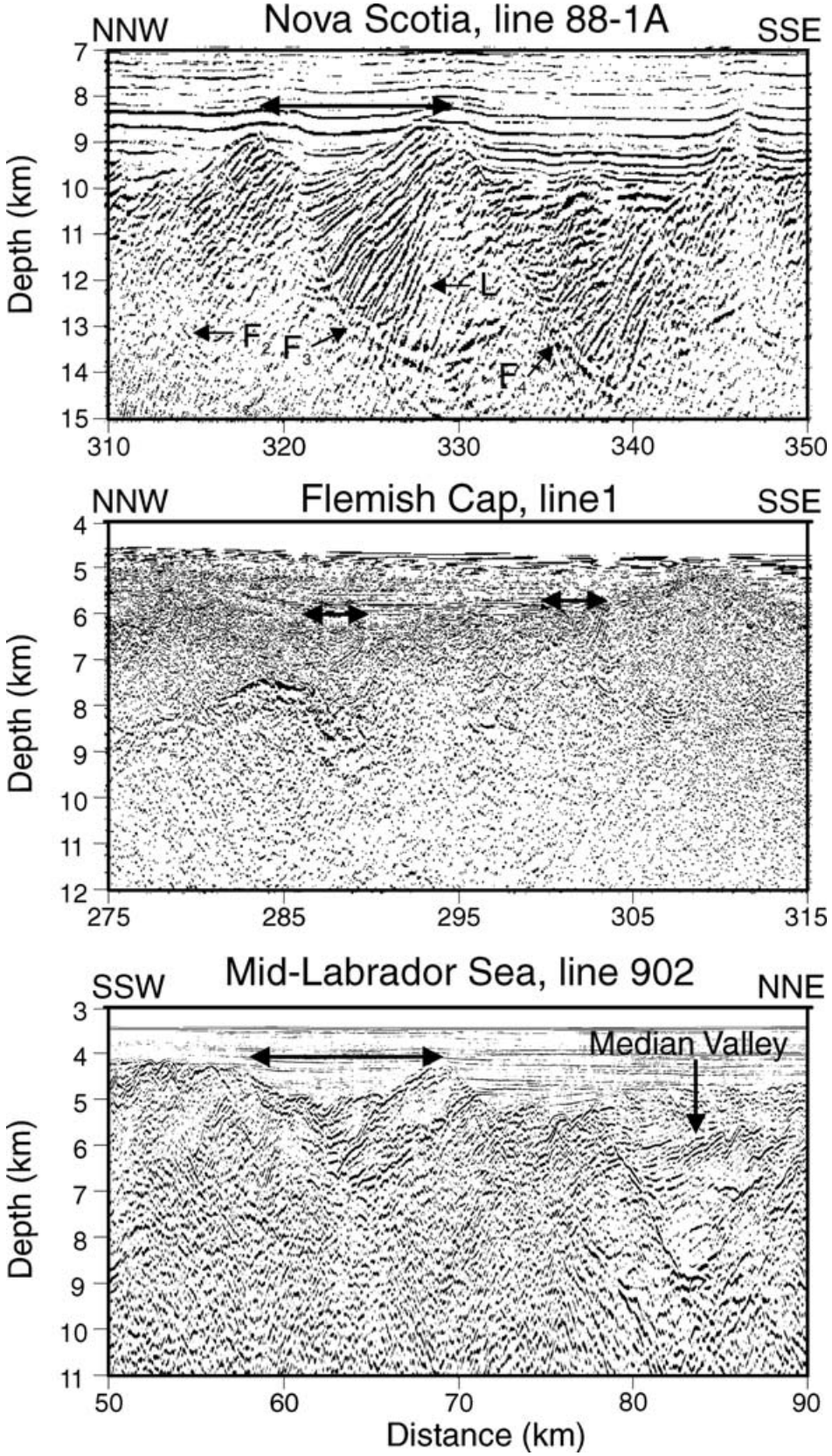

Figure 12. Basement topography and internal reflectivity of the faulted basement blocks along 88-1A (upper panel, after Keen *et al.* 1991b) compared with line 1 on the Newfoundland rifted margin (middle panel, after Hopper *et al.* 2004) and mid-Labrador Sea MCS profile 902 (bottom, after Srivastava & Keen 1995; Louden *et al.* 1996). Distances are referenced to the coincident velocity models. Double-arrows mark the location and horizontal region of basement structures, discussed in the text. Features marked by letters are F_2-F_4, listric normal faults bounding the highly faulted basement blocks; L, landward-dipping reflectors.

sufficiently long periods. The basement features of the FB are also different from those observed elsewhere on oceanic crust. In Fig. 12, the FB blocks along 88-1A (Keen *et al.* 1991b) are compared with those observed on the Newfoundland rifted margin (Hopper *et al.* 2004) and mid-Labrador Sea (Srivastava & Keen 1995). The basement blocks observed on Line 2 (top, Fig. 12) are segmented and rotated by uniformly seaward-dipping faults (F_1-F_4, Figs 12), creating half-grabens up to ∼10 km across. Within the FB, landward-dipping reflectors (L, Figs 12) fan against the listric faults with the steepest dip angle greater than 40°. Across the Newfoundland rifted margin off Flemish Cap, Hopper *et al.* (2004) identified a region where volcanism dominated seafloor spreading. However, this example shows no faulting pattern bounding the oceanic basement blocks, and no fanning sequences of volcanic overflows within the separate volcanic episodes (middle, Fig. 12). Across the abandoned median valley of the Mid-Labrador Sea (Srivastava & Keen 1995), which is rifting-dominated oceanic crust, even though the horizontal scale of the individual overflows (bottom, Fig. 12) is close to that observed on Line 2, no fanning reflectors are imaged within the volcanic units. This distinguishes the basement structures observed along Line 2 from those observed on oceanic crust across the Newfoundland rifted margin off Flemish Cap and the extinct spreading centre of the mid-Labrador Sea.

5.2.2 Oceanic crust

The upper basement layer seawards of the FB is interpreted to be oceanic crust (Fig. 8). The *P*-wave velocities of 5.6–6.0 km s^{-1} are within the global velocity range for layer 2 (White *et al.* 1992). In addition, a series of faults are imaged on MCS line 89-11, penetrating into the basement (F_5-F_9, Fig. 13). These faults result in a variable crustal thickness and irregular basement relief (e.g. H and N in Fig. 13), which is a typical representation of oceanic basement created by slow seafloor spreading (White *et al.* 1994). The initial thickness just seawards of the FB is 3–3.5 km; it reduces to 2–3 km at the seaward end of the model. The thickness variation suggests that this layer may have been affected by faulting (see faults F_5 and F_6 in Fig. 13) and small-scale fracturing that would reduce the velocities at depth.

An alternative interpretation is that this layer could be exhumed upper mantle. Such a layer was observed on Line 1 across the northern Nova Scotia margin (Funck *et al.* 2004). However, the exposed serpentinized mantle layer on Line 1 is characterized by flat basement topography and constant thickness without major faults. The rough basement relief and the presence of major faults in the basement do not support an interpretation of an exposed mantle layer for the central Nova Scotia margin. In summary, initial oceanic crust accretes seawards of the highly thinned continental crust, with a sharp COB (Fig. 13) in the upper part of the OCT zone.

5.2.3 High-velocity lower crustal layer

The HVLC layer beneath the interpreted oceanic basement described above has velocities of 7.25–7.4 km s^{-1}, which decrease to 6.95–7.3 km s^{-1} at the seaward end of the model. The initially ∼1 km thick layer thickens gradually seawards to about 3.5 km. The seaward portion has velocities within the global range of 6.7–7.2 km s^{-1} for oceanic layer 3 (White *et al.* 1992). The observed velocities at the landward side do not fall into the normal range of layer 3, although similar velocities are interpreted as layer 3 across the Labrador Sea (Osler & Louden 1995).

The atypically high velocities suggest that the HVLC layer may consist of a mixture of mantle with some frozen mafic melt. Such a mix may result from incomplete separation of rising melt from mantle when surface cooling freezes the upwelling melt in the mantle. This is consistent with the mafic and ultramafic mix models where mantle material is incorporated within the lower oceanic crust at slow spreading rates (Cannat 1993; Sleep & Barth 1997). The incomplete separation of rising melt reduces the bulk velocity of the upper mantle or seismically determined 'lower crust'. The seaward reduction of velocity is attributed to the increasing amount of separation of upwelling melt from ultramafic mantle.

Subsequent serpentinization may have further reduced the velocities and increased the velocity gradient as the amount of serpentinization reduces with depth. The faults through the episodic volcanic flows (F_5-F_9, Fig. 13) enable seawater to penetrate into and serpentinize the uppermost mantle. Provided the velocity reduction is entirely due to mantle serpentinization, the degree of serpentinization inferred from the observed *P*-wave velocities is <25 per cent (Miller & Christensen 1997).

Another possible hypothesis for the origin of the anomalous velocities is a high temperature of partial melting followed by fractionation. However, this interpretation is not consistent with the reduced thickness of the HVLC layer. To create the anomalously high velocity (7.25–7.4 km s^{-1}), a temperature anomaly of ∼300° C would be required in the mantle, and more than 20 km thickness of igneous crust would be expected due to passive upwelling (White & McKenzie 1989; Korenaga *et al.* 2000). In addition, the depth (<5 km beneath basement surface) of the HVLC layer is much shallower than the estimated depth of 20–35 km for the top of partial melting and fractionation below slow spreading mid-ocean ridge (Herzberg 2004).

5.2.4 PSM layer

The bottom layer of the OCT zone is also an anomalous velocity layer. Its velocities (7.6–7.95 km s^{-1}), compared to measurement of rock samples (Holbrook *et al.* 1992; Christensen & Mooney 1995), fall into a range of possible rocks such as serpentinized peridorite, underplated material, or a mix of intrusion and mantle material. The observations discussed below, however, are more consistent with an interpretation of partially serpentinized upper mantle.

The PSM layer is first observed beneath the highly thinned continental crust where a series of faults penetrate through the overlying crust (F_1-F_4, Fig. 13). Rheological models show that mantle serpentinization occurs when the entire overlying crust lies within the brittle regime (Pérez-Gussinyé & Reston 2001), which is evidenced here by the major faults. These major faults allow circulation of seawater down to the uppermost mantle, by which the mantle rocks become serpentinized. Further seawards, an increasingly thinner PSM layer coincides with an increasingly thicker overlying basement (F_5-F_9, Fig. 13). The PSM layer pinches out eventually at ∼480 km when the overlying basement layer thickens to ∼6 km. Such a PSM layer underneath oceanic basement has been documented along the Flemish Cap margin (Funck *et al.* 2003).

The reduced velocities (7.6–7.95 km s^{-1}) in the PSM layer indicate <12 per cent of serpentinization (Miller & Christensen 1997). The *P*-wave velocities of the PSM in the OCT zone are well constrained, but its boundary with the underlying unaltered mantle is poorly parametrized (S, Fig. 9). This indicates that the boundary more likely represents a transition in the upper mantle from a relatively higher velocity gradient to a lower gradient with no velocity discontinuity.

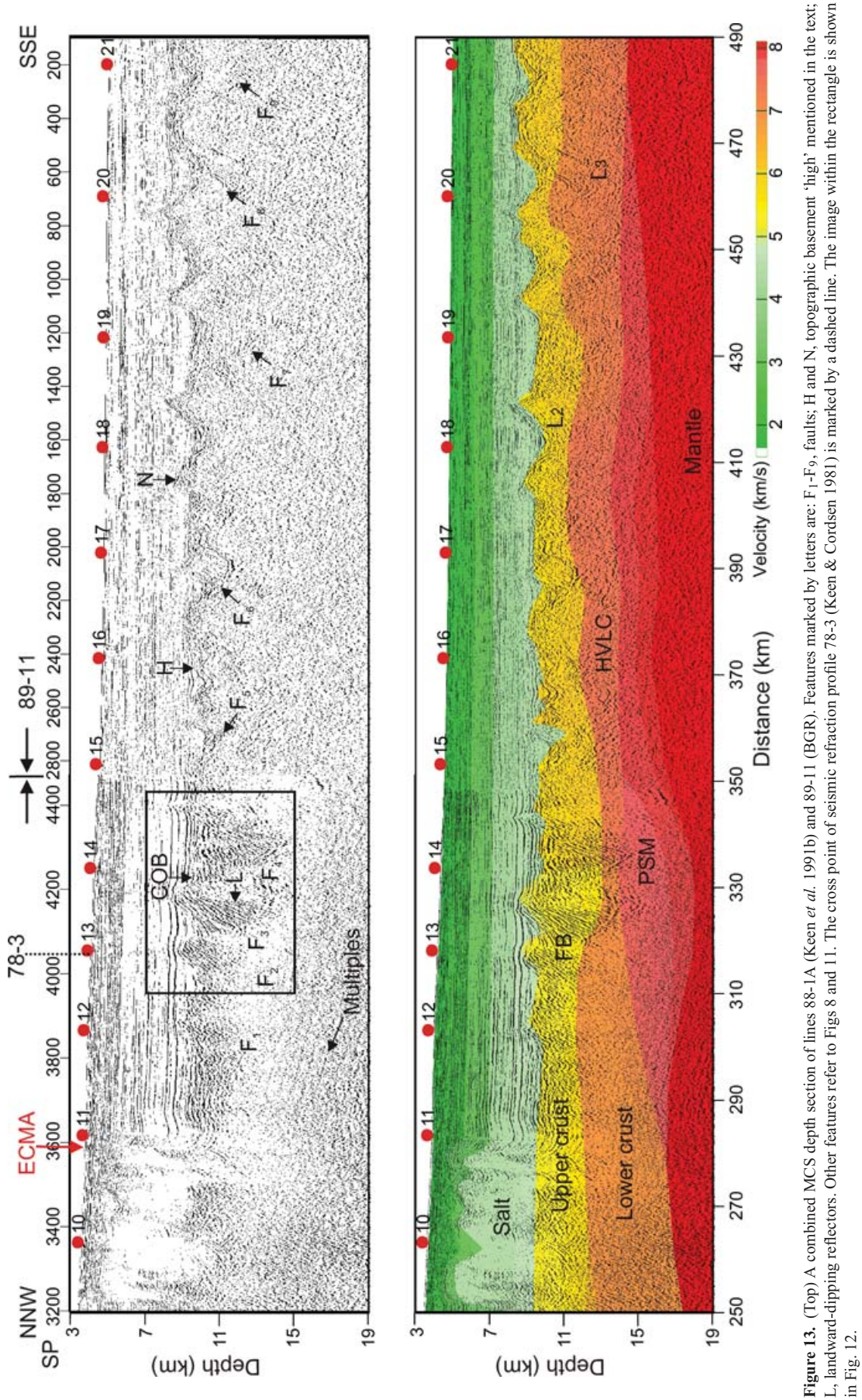

Figure 13. (Top) A combined MCS depth section of lines 88-1A (Keen *et al.* 1991b) and 89-11 (BGR). Features marked by letters are: F_1-F_9, faults; H and N, topographic basement 'high' mentioned in the text; L, landward-dipping reflectors. Other features refer to Figs 8 and 11. The cross point of seismic refraction profile 78-3 (Keen & Cordsen 1981) is marked by a dashed line. The image within the rectangle is shown in Fig. 12.

We compare the PSM with similar layers elsewhere. The velocities and gradients of this layer are similar to those of the bottom layer in the OCT zone across the southern Iberia Abyssal Plain, which are 7.6 km s^{-1} and ~0.1 s^{-1} for velocity and gradient, respectively (Chian *et al.* 1999; Dean *et al.* 2000). The width and thickness of the lower layer are comparable, about 170 and 4 km, respectively, for these two margins. The velocities (6.4–7.7 km s^{-1}) for the Labrador Sea-SW Greenland conjugates are lower than that observed along Line 2, and the thickness of the former (4–5 km; Chian *et al.* 1995a) is relatively greater than that of Line 2 (~4 km). However, a higher velocity gradient (~0.3 s^{-1}) occurs for the Labrador Sea-SW Greenland margin conjugates, suggesting a higher degree of serpentinization; the overlying basement is also thinner (< 2 km; Chian *et al.* 1995a,b).

Since the velocities also fall within the range of magmatically underplated material observed on volcanic margins, an alternative interpretation might be an underplated layer. This hypothesis is not favoured by comparing the velocity model and magnetic anomalies observed here with those for volcanic margins elsewhere. Firstly, the extremely high velocities of 7.6–7.95 km s^{-1}, if attributed to underplating, would require an extremely high melting temperature. The high temperature would produce a large amount of magmatic intrusion and underplating, such as the 12- to 15-km-thick underplated layer beneath the US East Coast margins (Holbrook & Kelemen 1993; Kelemen & Holbrook 1995). In contrast, the PSM layer on Line 2 is only ~4 km thick. In addition, this layer is ~200 km across and its location is more than 100 km away from the hinge line. Both of these observations contradict crustal models for the US East Coast margins where a 100-km-wide layer of underplated rocks is located underneath the outer shelf (Holbrook & Kelemen 1993). Furthermore, the underplated layer associated with SDR sequence along the US margin is observed beneath the ECMA (Talwani *et al.* 1995; Talwani & Abreu 2000), while the PSM layer on Line 2 begins seawards of the ECMA and there are no observations of SDR sequences (Fig. 13). Thus, the bottom layer along this margin segment is not related to the ECMA as it is on the US East Coast. Paleomagnetic data also suggest that the Triassic magmatism on land is only a brief coeval magmatic event which ceased well before continental break-up (Marzoli *et al.* 1999). Based on the above comparisons, we conclude that the bottom layer observed along Line 2 is not produced by underplated rocks.

Another hypothesis is that the PSM layer could be a mix of mafic intrusion and unserpentinized mantle. This would occur if melt is frozen in the mantle by surface cooling, similar to the explanation of the HVLC layer. However, thermal models suggest that frozen melt due to surface cooling mostly occurs at shallow depths (e.g. ≤5 km) below the seafloor (Sleep & Barth 1997). Furthermore, ultraslow mid-ocean ridge, such as the Gakkel Ridge (Jokat *et al.* 2003) and Southwest Indian Ridge (Minshull & White 1996; Muller *et al.* 1999), do not demonstrate a reduced velocity in the off-axis mantle. Therefore, such a hypothesis does not explain the reduced mantle velocities in the PSM layer.

5.3 Along-strike variations of margin

Fig. 14 compares the velocity model along Line 2 with that for Line 1 (Funck *et al.* 2004). Both models indicate a non-volcanic character

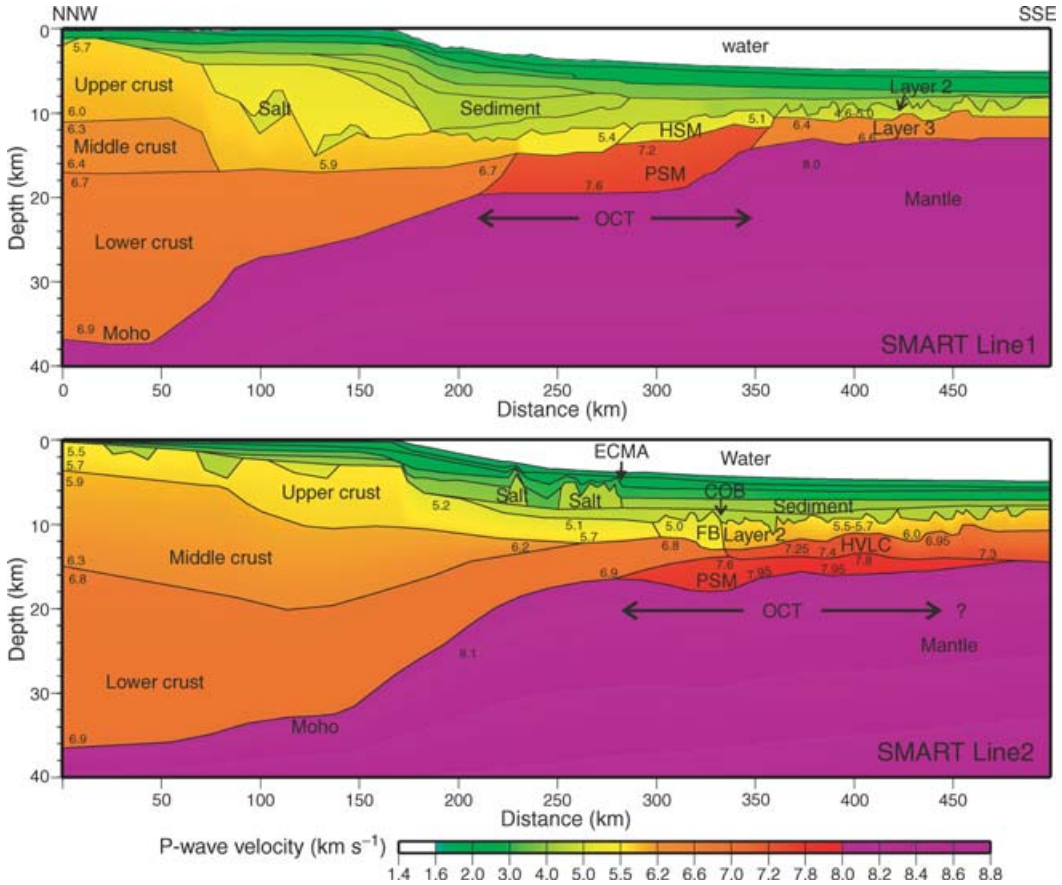

Figure 14. A comparison of velocity models along Line 1 (upper panel, Funck *et al.* 2004) and Line 2 (lower panel). *P*-wave velocities are indicated by a colour scalar and numbers in the models (in km s^{-1}). Abbreviation: HSM, exhumed and highly serpentinized upper mantle. Other features refer to Fig. 8.

for the northeastern part of the Nova Scotia margin. Nonetheless, significant differences occur during the continental extension and the transition to seafloor spreading along the two margin segments. In the following sections, variations in crustal structure during the rift-to-drift transition and syn-rift crustal thinning are compared between the two velocity models and correlated with regional magnetic anomalies.

5.3.1 Rift-to-drift transition

The velocity models for Lines 1 and 2 show that both margin segments contain an OCT zone. The OCT zone of Line 2 consists of a PSM layer, overlain by highly faulted continental crust in the northwest and oceanic crust in the southeast. Thin oceanic crust forms immediately seawards of continental break-up. In contrast, the OCT zone of Line 1 comprises a 70-km-wide upper layer of exhumed and highly serpentinized mantle (HSM) overlying a PSM layer. This suggests that at the time of break-up, limited magma was generated across the central margin segment while no melt was created across the northern Nova Scotia margin. The PSM layer in the OCT zone of Line 1 is ∼6 km thick with velocities of 7.2–7.6 km s^{-1}; the corresponding layer for Line 2 is less than 4 km thick with higher velocities of 7.6–7.95 km s^{-1}. This suggests a relatively low degree of mantle serpentinization along Line 2, and an increasingly higher percentage of serpentinized mantle towards Line 1. The oceanic crust for Line 1 is only ∼4 km thick compared with 7.1±0.8 km for normal oceanic crust (White *et al.* 1992), indicating a magma-starved margin after initiation of seafloor spreading. Along Line 2, although the initial oceanic crust could be ∼4 km thick considering the mantle material incorporated to the HVLC layer, the oceanic crust at the seaward end has a more normal thickness of 5–7 km, which is 2–3 km thicker than on Line 1. The thickness variation also implies an increase of magma supply from the northern margin to the central margin. The preliminary results for Line 3 show an underplated lower crustal layer (Dehler *et al.* 2004) coinciding with the SDR sequence that is observed nearby on MCS profiles 89-3 and 4 (Keen & Potter 1995a). This further suggests a continuing increase of volcanism towards the southern Nova Scotia margin, where the margin eventually changes its character from a non-volcanic margin to a volcanic margin.

5.3.2 Syn-rift crustal thinning

The thinning of the continental crust calculated from the velocity models in Fig. 15 also presents different features across the two margin segments. For Line 2, the continental crust underwent a few kilometres (∼5 km) of gradual thinning over the outer continental shelf, followed by a rapid thinning across the continental slope into the ocean basin (lower panel, Fig. 15). The limited initial crustal thinning for the Lahave Platform was not able to counteract the uplift resulting from the thinning of subcrustal lithosphere predicted by subsidence analysis (Keen & Beaumont 1990) and therefore, there was no space beneath the shelf edge area to accommodate thick sediments. In contrast, the continental crust along Line 1 is dramatically thinned right from the onset of rifting, followed by a gradual thinning to the ocean basin (upper panel, Fig. 15). The abrupt crustal thinning across the northern margin has given rise to a rapid subsidence and formation of the deep Sable Basin seawards of the hinge line.

The results are basically in agreement with estimates of thermal-mechanical modelling for this margin (Keen & Beaumont 1990).

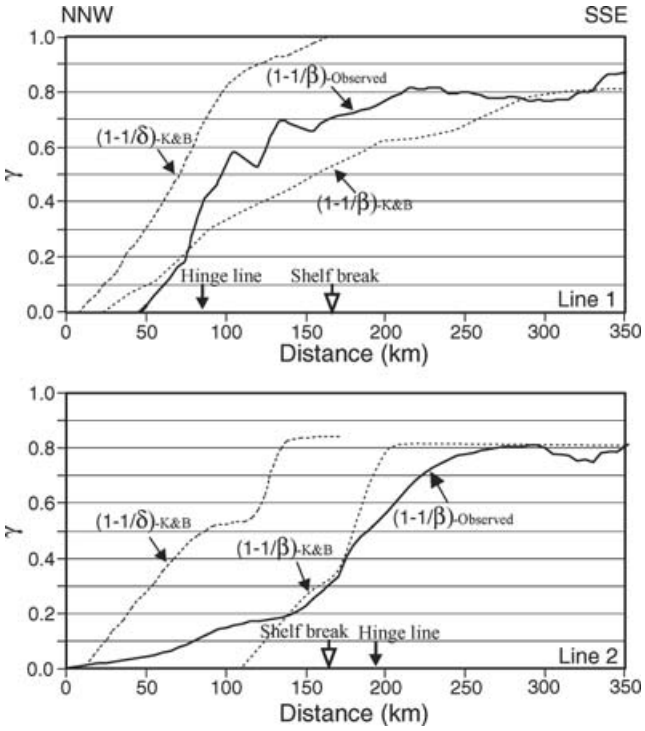

Figure 15. Comparison of model results with estimates of the thermal-mechanical models (Keen & Beaumont 1990) for Line 1 (upper panel) and Line 2 (lower panel). β and δ are the equivalent crustal and subcrustal thinning factors (1-1/β) and (1-1/δ), respectively. γ refers to either (1-1/β) or (1-1/δ) indicated by arrows. K&B, thermal-mechanical model of Keen & Beaumont (1990). Solid thick arrows mark the location of hinge lines. Open arrows indicate the location of shelf break.

The thermal-mechanical models are primarily based on subsidence analysis of exploratory well data. These models predict a non-uniform thinning of crustal and subcrustal lithosphere across the Lahave Platform, which produced uplift and erosion, and a more uniform thinning across the Scotian Basin, which created subsidence at the onset of rifting (Fig. 15). However, the velocity model shows that the crustal thinning along Line 2 occurs about 100 km farther landward compared to the results of the thermal-mechanical models (lower panel, Fig. 15). Provided that the result of the subcrustal lithospheric thinning (δ) is correct, we use the δ value and the crustal thinning (β) obtained from this experiment to calculate the subsidence through the non-uniform extension model of Royden & Keen (1980). The resulting maximum uplift of ∼0.75 km across the central Nova Scotia margin is significantly less than estimates of ∼2 km from the thermal-mechanical model (Keen & Beaumont 1990). In comparison, the crustal thinning for Line 1 starts 20–30 km further seawards and appears to be more rapid and abrupt over the slope area (upper panel, Fig. 15), indicating a deeper basin seawards of the hinge line compared to analysis of Keen & Beaumont (1990).

5.3.3 Comparison with regional magnetic anomaly

Selected magnetic profiles from the US East Coast to the northern Nova Scotia margin are shown in Fig. 16. The ECMA along the US East Coast margin is a broad anomaly of ±300 nT, which is thought to mark an igneous wedge created by voluminous magma intrusion and extrusion at the COB (Kelemen & Holbrook 1995; Talwani *et al.* 1995). This anomaly becomes narrower and sharper as it approaches the southwest Nova Scotia margin (Fig. 16e–i),

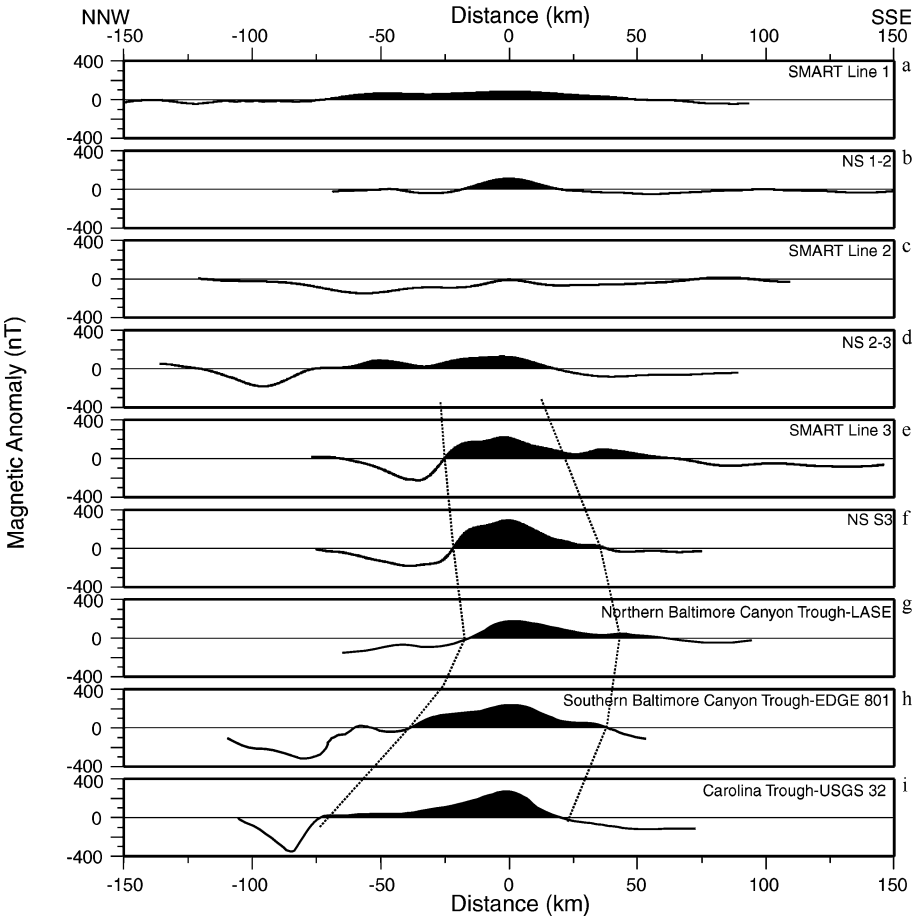

Figure 16. Selected magnetic profiles across the East Coast margin of North America. The upper six profiles (a–f) are taken from Oakey & Dehler (2004) and their locations are shown in Fig. 17. The lowest three sections (g–i) are after Talwani *et al.* (1995). The distances are with respect to the peak anomaly of ECMA (0 km). The positive anomalies are filled with black. The relative widths of the ECMA are defined by two dotted lines.

suggesting a narrower zone of volcanism. Further north of this region, the magnetic anomaly becomes broader and the amplitude decreases [Figs 16a–d]. The along-strike magnetic signature implies that the anomaly source changes its character between Line 3 and profile NS 2–3 (Figs 16 and 17). The weak anomalies north of this region suggest that igneous material was not emplaced. This is consistent with the velocity models for Line 2 and Line 1 where no underplated material was identified within the transition zones.

The ECMA with reduced amplitude may be caused by the transition from highly thinned continental crust to serpentinized mantle rocks with different degrees of serpentinization. The ECMA along most of the margin up to MCS line 89-1 is roughly coincident with the distribution of the autochthonous salt (Shimeld 2004), suggesting that the underlying basement should be continental. The velocity models show that the landward extent of the OCT zone on Lines 1 and 2 is roughly consistent with the seaward limit of the ECMA (Fig. 17). Further offshore, a 'speckled' magnetic pattern correlates with oceanic crust. This suggests that the onset of the serpentinized transition zone is consistent with regional magnetic patterns. The subdued longer wavelength anomalies between the ECMA and the 'speckled' pattern are associated with either highly thinned continental crust (Line 2) or exposed and highly serpentinized upper mantle (Line 1, Funck *et al.* 2004). Southwest of Line 2, the magnetic anomaly between the ECMA and the 'speckled' pattern is dominantly negative. A preliminary model for Line 3 indicates oceanic crust underlies most of the negative anomaly at the seaward end of the line (Dehler *et al.* 2004).

6 CONCLUSIONS

We have presented a *P*-wave velocity model derived from seismic refraction data across the central Nova Scotia margin. The crustal structure is divided into rifted continental crust, an OCT zone and oceanic crust. The maximum thickness of the continental crust is ∼36 km and it thins seawards to 5–6 km. Most of the thinning occurs over the slope region, while ∼5 km of crustal thinning occurs beneath the outer shelf. The FB are interpreted as the seaward-most continental fragments. The OCT zone contains a PSM layer, which extends from beneath the FB and ∼200 km farther seawards beneath initial oceanic crust. Oceanic crust with normal thickness of 5–7 km is observed at the seaward end of the line.

The results suggest several modifications to earlier interpretations. First of all, the thinned continental crust extends up to a highly faulted basement structure, which was previously interpreted to be oceanic. With the new interpretation, the COB is moved ∼50 km farther seawards. Furthermore, the velocity model shows that the initial continental thinning along Line 2 occurs ∼100 km farther landwards, compared to results of earlier thermal-mechanical models.

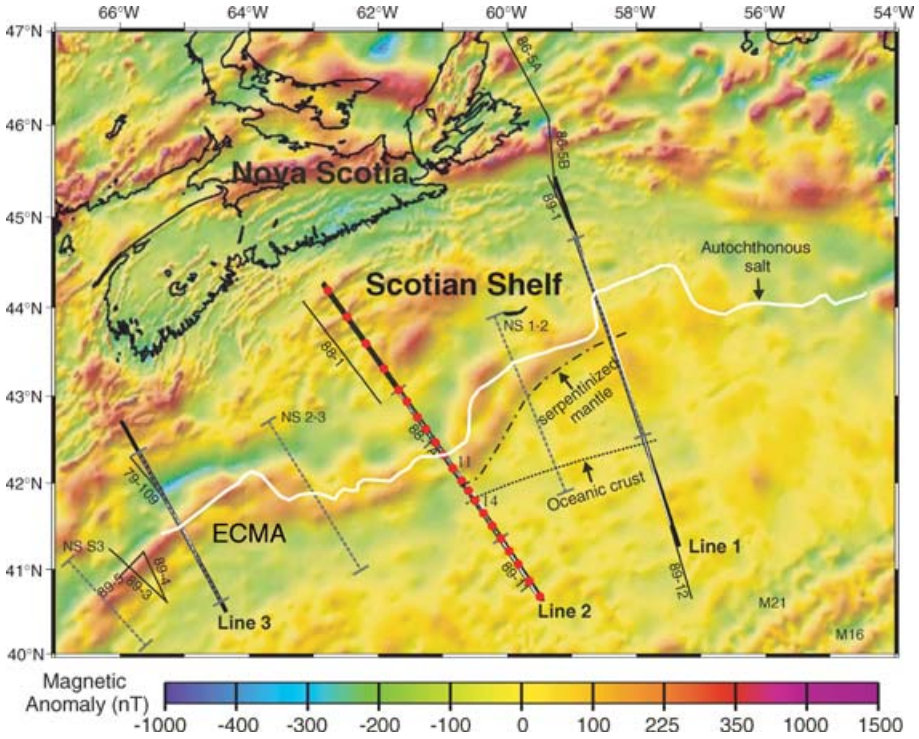

Figure 17. Magnetic anomaly map for the Nova Scotia margin and surrounding areas. Magnetic data are taken from Oakey & Dehler (2004). Bold solid lines represent the shot lines of the experiment with red circles indicating the location of OBS along Line 2. Other reflection seismic lines in the area are shown as thin black lines (see Fig. 1 for references). Dashed lines are magnetic profiles extracted from the magnetic map and shown in Fig. 16. OBS 11 and OBS 14 are annotated for reference. The thick white line marks the seaward boundary of the autochthonous salt (Shimeld 2004). The dot-dashed line marks the landward limit of the serpentinized mantle. The dotted line marks the landward limit of the 'speckled' magnetic anomaly pattern, which is roughly coincident with the onset of the oceanic crustal accretion in this area. The magnetic lineation at the right lower corner represents magnetic anomalies M21 and M16 (Barrett & Keen 1976; Klitgord & Schouten 1986).

The velocity model shows no evidence for a magmatic underplated layer beneath the continental crust, suggesting primarily non-volcanic rifting across the central Nova Scotia margin. The high-amplitude of the magnetic anomaly related to the excessive volcanism south of the Nova Scotia margin does not extend further north along most of the margin. Compared to the magma-starved margin segment along Line 1 to the northeast, the results on Line 2 indicate a normal melt supply after continental break up. Although the melt generation along these margin segments farther to the south may have been affected by extensive volcanism, we suggest that the entire Nova Scotia margin, except for the southernmost part near Georges Bank, is non-volcanic in character.

ACKNOWLEDGMENTS

We thank the scientists, technicians and all individuals onboard the CCGS HUDSON who helped carry out the seismic experiment in 2001. The experiment was funded by the Natural Sciences and Engineering Research Council of Canada (NSERC), the Geological Survey of Canada and the Danish National Research Foundation. Seismic line 89-11 was collected as part of a collaborative program between the Geological Survey of Canada and the German Federal Agency of Geosciences and Natural Resources (BGR). We are grateful to Tim Minshull, Tim Reston and Isabelle Contrucci for their comments and valuable suggestions on the manuscript. This is Geological Survey of Canada contribution number 2005124.

REFERENCES

Barr, S.M. & Raeside, R.P., 1989. Tectono-stratigraphic terranes in Cape Breton Island, Nova Scotia: implications for the configuration of the northern Appalachian orogen, *Geology,* **17,** 822–825.

Barrett, D.L. & Keen, C.E., 1976. Mesozoic magnetic lineations, the magnetic quiet zone, and sea floor spreading in the northwest Atlantic, *J. geophys. Res.,* **81,** 4875–4884.

Benn, K., Horne, R.J., Kontak, D.J., Pignotta, G.S. & Evans, N.G., 1997. Syn-Acadian emplacement model for the South Mountain batholith, Meguma Terrane, Nova Scotia: magnetic fabric and structural analyses, *Geological Society of America Bulletin,* **109,** 1279–1293.

Bown, J.W. & White, R.S., 1995. Effect of finite extension rate on melt generation at rifted continental margins, *J. geophys. Res.,* **100,** 18 011–18 029.

Cannat, M., 1993. Emplacement of mantle rocks in the seafloor at mid-ocean ridges, *J. geophys. Res.,* **98,** 4163–4172.

Chian, D., Louden, K.E. & Reid, I., 1995a. Crustal structure of the Labrador Sea conjugate margin and implications for the formation of nonvolcanic continental margins, *J. geophys. Res.,* **100,** 24 239–24 253.

Chian, D., Keen, C., Reid, I. & Louden, K.E., 1995b. Evolution of non-volcanic rifted margins: new results from the conjugate margins of the Labrador Sea, *Geology,* **23,** 589–592.

Chian, D., Louden, K.E., Minshull, T.A. & Whitmarsh, R.B., 1999. Deep structure of the ocean-continent transition in the southern Iberia Abyssal Plain from seismic refraction profiles: Ocean Drilling Program (Legs 149 and 173) transect, *J. geophys. Res.,* **104,** 7443–7462.

Christensen, N.I. & Mooney, W.D., 1995. Seismic velocity structure and composition of the continental crust: a global view, *J. geophys. Res.,* **100**(B6), 9761–9788.

Dean, S.M., Minshull, T.A., Whitmarsh, R.B. & Louden, K.E., 2000. Deep structure of the ocean-continent transition in the southern Iberia Abyssal Plain from seismic refraction profiles: The IAM-9 transect at 40°20′N, *J. geophys. Res.,* **105,** 5859–5885.

Dehler, S.A., Keen, C.E., Funck, T., Jackson, H.R. & Louden, K.E., 2004. The limit of volcanic rifting: A structural model across the volcanic to non-volcanic transition off Nova Scotia, *EOS, Trans. Am. geophys. Un.,* **85**(17), Jt. Assem. Suppl., Abstract T31D-04.

Funck, T., Hopper, J.R., Larsen, H.C., Louden, K.E., Tucholke, B.E. & Holbrook, W.S., 2003. Crustal structure of the ocean-continent transition at Flemish Cap: seismic refraction results, *J. geophys. Res.,* **108**(B11), 2531, doi:10.1029/2003JB002434.

Funck, T., Jackson, H.R., Louden, K.E., Dehler, S.A. & Wu, Y., 2004. Crustal structure of the northern Nova Scotia rifted continental margin (Eastern Canada), *J. geophys. Res.,* **109,** B09102, doi:10.1029/2004JB003008.

Herzberg, C., 2004. Partial crystallization of mid-ocean ridge basalts in the crust and mantle, *J. Petrol.,* **45,** 2389–2405.

Holbrook, W.S. & Kelemen, P.B., 1993. Large igneous province on the US Atlantic margin and implications for magmatism during continental breakup, *Nature,* **364,** 433–436.

Holbrook, W.S., Mooney, W.D. & Christensen, N.I., 1992. The seismic velocity structure of the deep continental crust, in *Continental Lower Crust*, pp. 1–43, eds Fountain, D.M., Arculus, R. & Kay, R., Elsevier, Amsterdam.

Hopper, J.R., Funck, T., Tucholke, B.E., Larsen, H.C., Holbrook, W.S., Louden, K.E., Shillington, D. & Lau, H., 2004. Continental breakup and the onset of ultraslow seafloor spreading off Flemish Cap on the Newfoundland rifted margin, *Geology,* **32**(1), 93–96, doi:10.1130/G19694.1.

Jokat, W., Ritzmann, O., Schmidt-Aursch, M.C., Drachev, S., Gauger, S. & Snow, J., 2003. Geophysical evidence for reduced melt production on the Arctic ultraslow Gakkel mid-ocean ridge, *Nature,* **423,** 962–965.

Keen, C.E. & Beaumont, C., 1990. Geodynamics of rifted continental margins, in *Geology of the Continental Margin of Eastern Canada*, pp. 393–472, eds Keen, M.J. & Williams, G.L., Geological Survey of Canada, Geology of Canada, No. 2.

Keen, C.E. & Cordsen, A., 1981. Crustal structure, seismic stratigraphy, and rift processes of the continental margin off eastern Canada: ocean bottom seismic refraction results off Nova Scotia, *Can. J. Earth Sci.,* **18,** 1523–1538.

Keen, C.E., Kay, W.A., Keppie, D., Marillier, R., Pe-Piper, G. & Waldron, J.W.F., 1991a. Deep seismic reflection data from the Bay of Fundy and marine: tectonic implication for the northern Appalachian, *Can. J. Earth Sci.,* **28,** 1096–1111.

Keen, C.E., MacLean, B.C. & Kay, W.A., 1991b. A deep seismic reflection profile across the Nova Scotia continental margin, offshore eastern Canada, *Can. J. Earth Sci.,* **28,** 1112–1120.

Keen, C.E. & Potter, P., 1995a. The transition from a volcanic to nonvolcanic rifted margin off eastern Canada, *Tectonics,* **14,** 359–371.

Keen, C.E. & Potter, P., 1995b. Formation and evolution of the Nova Scotian rifted margin: Evidence from deep seismic reflection data, *Tectonics,* **14,** 918–932.

Kelemen, P.B. & Holbrook, W.S., 1995. Origin of thick, high-velocity igneous crust along the US East Coast Margin, *J. geophys. Res.,* **100**(B7), 10 077–10 094.

Keppie, J.D., 1989. Northern Appalachian terranes and their accretionary history, in *Terranes in the circum-Atlantic Paleozoic Orogens*, **Vol. 230,** pp. 159–192, ed. Dallmeyer, R.D., Geological Society of America, Special Paper.

Klitgord, K.D. & Schouten, H., 1986. Plate kinematics of the central Atlantic, in *The Geology of North America, Volume M, The Western North Atlantic Region*, pp. 351–378, eds Vogt P.R. & Tucholke, B.E., Geological Society of America, Boulder, Colo.

Korenaga, J., Holbrook, W.S., Kent, G.M., Kelemen, P.B., Detrick, R.S., Larsen, H.C., Hopper, J.R. & Dahl-Jensen, T., 2000. Crustal structure of the Southeast Greenland margin from joint refraction and reflection seismic tomography, *J. geophys. Res.,* **105,** 21 591–21 614.

Loncarevic, B.D. et al., 1994. Sonography of a glaciated continental shelf, *Geology,* **22,** 747–750.

Louden, K.E. & Chian, D., 1999. The deep structure of non-volcanic rifted continental margins, *Phil Trans. Roy. Soc. Lond., Ser., A.,* **357,** 767–804.

Louden, K.E., Osler, J.C., Srivastava, S.P. & Keen, C.E., 1996. Formation of oceanic crust at slow spreading rates: New constraints from an extinct spreading center in the Labrador Sea, *Geology,* **24,** 771–774.

Ludwig, W.J., Nafe, J.E. & Drake, C.L., 1970. Seismic refraction, in *The Sea, New concepts of the sea floor evolution*, pp. 53–84, ed. Maxwell, A.E., Wiley-intersci., New York.

Lutter, W.J. & Nowack, R.L., 1990. Inversion for crustal structure using reflections from the PASSCAL Ouachita experiment, *J. geophys. Res.,* **95,** 4633–4646.

MacLean, B.C., 1991. Structure and isopach 1: depth to pre-Mesozoic basement and oceanic layer 2; In *East Coast Basin Atlas Series: Scotian Shelf,* Atlantic Geoscience Centre, Geological Survey of Canada, 75.

Marillier, F., Keen, C.E., Stockmal, G.S., Quinlan, G., Williams, H., Colman-Sadd, S.P. & O'Brien, S.J., 1989. Crustal structure and surface zonation of the Canadian Appalachians: implications of deep seismic reflection data, *Can. J. Earth Sci.,* **26,** 305–321.

Marzoli, A., Renne, P.R., Piccirillo, E.M., Ernesto, M., Bellieni, G. & Min, A., De, 1999. Extensive 200-million-year-old continental flood basalts of the Central Atlantic Magmatic Province, *Science,* **284,** 616–618.

Miller, D.J. & Christensen, N.I., 1997. Seismic velocities of lower crustal and upper mantle rocks from the slow-spreading Mid-Atlantic Ridge, south of the Kane Transform zone (MARK), *Proc. Ocean Drill. Program Sci. Results,* **153,** 437–454.

Minshull, T.A. & White, R.S., 1996. Thin crust on the flanks of the slow-spreading Southwest Indian Ridge, *Geo. J. Int.,* **125,** 139–148.

Muller, M.R., Minshull, T.A. & White, R.S., 1999. Segmentation and melt supply at the Southwest Indian Ridge, *Geology,* **27,** 867–870.

National Geophysical Data Center, 1988. ETOPO-5 Bathymetry/Topography data, Data announcement 88-MG-02, National Oceanic and Atmospheric Administration, US Dept. of Commerce, Boulder, Colo.

Oakey, G.N. & Dehler, S.A., 2004. Atlantic Canada magnetic map series: Scotian shelf and surrounds, Open File Rep. 1814, Geological Survey of Canada, Calgary, Alb.

Osler, J. & Louden, K.E., 1995. Extinct spreading center in the Labrador Sea: crustal structure from a two-dimensional seismic refraction velocity model, *J. geophys. Res.,* **100,** 2261–2278.

Pérez-Gussinyé, M. & Reston, T.J., 2001. Rheological evolution during extension at nonvolcanic rifted margins: onset of serpentinization and development of detachments leading to continental breakup, *J. geophys. Res.,* **106,** 3961–3975.

Prosser, S., 1993. Rift-related linked depositional systems and their seismic expression, in *Tectonics and Seismic Sequence Stratigraphy*, Vol. 71, pp. 35–66, eds Williams, G.D. & Dobb, A., Geol. Soc. Spec. Publ. Lond.

Reid, I.D., 1994. Crustal structure of a nonvolcanic rifted margin east of Newfoundland, *J. geophys. Res.,* **99,** 15 161–15 180.

Royden, L. & Keen, C.E., 1980. Rifting process and thermal evolution of the continental margin of eastern Canada determined from subsidence curves, *Earth planet. Sci. Lett.,* **51,** 343–361.

Sahabi, M., Aslanian, D. & Olivet, J.-L., 2004. Un nouveau point de départ pour l'histoire de l'Atlantique central, *Comptes Rendus Geosciences,* **336,** 12, 1041–1052.

Salisbury, M.H. & Keen, C.E., 1993. Listric faults imaged in oceanic crust, *Geology,* **21,** 117–120.

Sandwell, D.T. & Smith, W.H.F., 1997. Marine gravity anomaly from Geosat and ERS 1 satellite altimetry, *J. geophys. Res.,* **102,** 10 039–10 054.

Sawyer, D.S., Whitmarsh, R.B., Klaus, A. & Shipboard Scientific Party, 1994. *Proceedings of the Ocean Drilling Program*, Initial Reports, 149, College Station, TX, 719.

Shimeld, J., 2004. A comparison of salt tectonic subprovinces beneath the Scotian Slope and Laurentian Fan, in *Salt Sediment Interactions and Hydrocarbon Prospectivity: Concepts, Applications, and Case Studies for the 21st Century*, 24th Annual Conference, eds Post, P., Olson, D., Lyons, K., Palmes, S., Harrison, P. & Rosen, N., Gulf Coast Section Society of Economic Paleontologists and Mineralogists Foundation (GCSSEPM), Houston, Texas (CD format).

Sleep, N.H. & Barth, G.A., 1997. The nature of oceanic lower crust and shallow mantle emplaced at low spreading rates, *Tectonophysics,* **279,** 181–191.

Srivastava, S.P. & Keen, C.E., 1995. A deep seismic reflection profile across the extinct Mid-Labrador Sea spreading center, *Tectonics,* **14,** 372–389.

Talwani, M. & Abreu, V., 2000. Inferences regarding initiation of oceanic crust formation from the US east coast margin and conjugate south Atlantic margins, in *Atlantic rifts and continental margins*, pp. 211–233, eds Mohriak, W. & Talwani, M., American geophysical Union, Geophysical Monograph 155, Washington, DC.

Talwani, M., Worzel, J.L. & Landisman, M., 1959. Rapid gravity computations for two-dimensional bodies with application to the Mendocino submarine fracture zone, *J. geophys. Res.,* **64,** 49–59.

Talwani, M., Ewing, J., Sheridan, R.E., Holbrook, W.S. & Glover, L. III., 1995. The EDGE experiment and the US Coast Magnetic Anomaly, in NATO/ARW Series book *Rifted Ocean-Continent Boundaries*, pp. 155–181, eds Banda, E., Talwani, M. & Torne, M., Amsterdam: Kluwer.

Wade, J.A., 1981. Geology of the Canadian Atlantic margin from Georges Bank to the Grand Banks, in *Geology of the North Atlantic Borderlands*, pp. 447–460. eds Kerr, J.Wm. & Ferguson, A.J., Canadian Society of Petroleum Geologists, Memoir 7.

Wade, J.A. & MacLean, B.C., 1990. The geology of the southeastern margin: aspects of the geology of the Scotian Basin from recent seismic and well data, in *Geology of the Continental Margin Eastern Canada*, pp. 167–238, eds Keen, M.J. & Williams, G.L., Geological Survey of Canada, Geology of Canada, No. 2.

Welsink, H.J., Dwyer, J.D. & Knight, R.J., 1989. Tectono-stratigraphy of the passive margin off Nova Scotia, in *Extensional tectonics and stratigraphy of the North Atlantic margin*, Vol., 46, pp. 215–231, eds Tankard, A.J. & Balkwill, H.R., American Association of Petroleum Geologists, Memoir.

White, R.S. & McKenzie, D.P., 1989. Magmatism at rift zones: the generation of volcanic continental margins and flood basalts, *J. geophys. Res.,* **94,** 7685–7729.

White, R.S., McKenzie, D. & O'Nions, K., 1992. Oceanic crustal thickness from seismic measurements and rare earth element inversions, *J. geophys. Res.,* **97,** 19 683–19 715.

White, R.S., McBride, J.H., Henstock, T.J. & Hobbs, R.W., 1994. Internal structure of Mesozoic oceanic crust, *Geology* **22,** 597–600.

Williams, H., 1979. Appalachian Orogen in Canada, *Can. J. Earth Sci.,* **16,** 792–807.

Zelt, C.A. & Forsyth, D.A., 1994. Modeling wide-angle seismic data for crustal structure: southeastern Grenville province, *J. geophys. Res.,* **99,** 11 687–11 704.

Zelt, C.A. & Smith, R.B., 1992. Seismic traveltime inversion for 2-D crustal structure, *Geophys. J. Int.,* **108,** 16–34.

APPENDIX A: ADDITIONAL RECORD SECTIONS WITH PHASE DESCRIPTION

Additional record sections are included in this appendix. OBS locations are shown in Fig 2. Labels are defined in Section 3.3. Other features refer to Fig. 3. The phases for each OBS are described as follows:

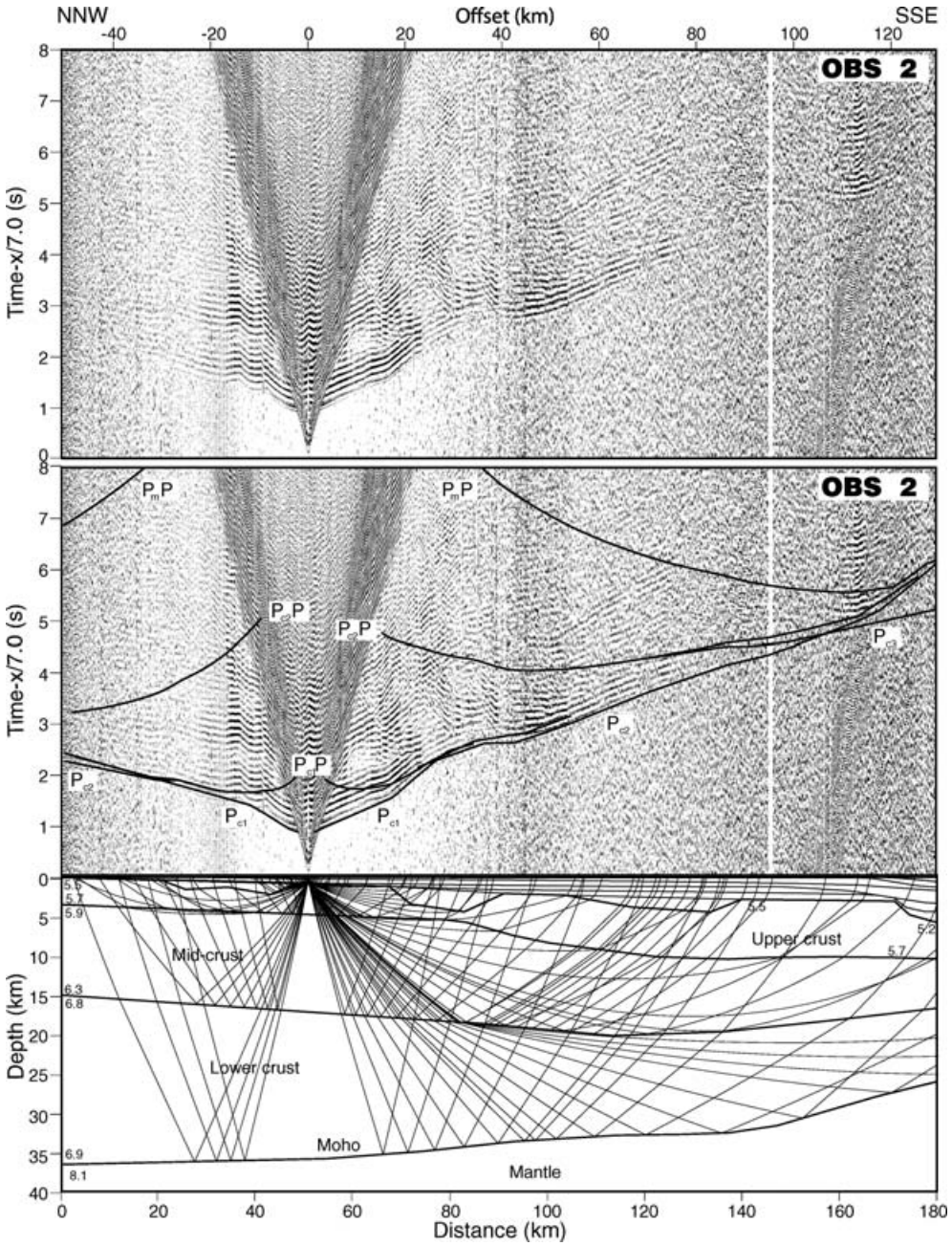

Figure A1. Record section for OBS 2 (hydrophone component). On this station, phases P_{c1} and P_{c2} are imaged, but P_{c3} is weak and difficult to identify. Reflections from these layers ($P_{c1}P$, $P_{c2}P$, P_mP) are weak.

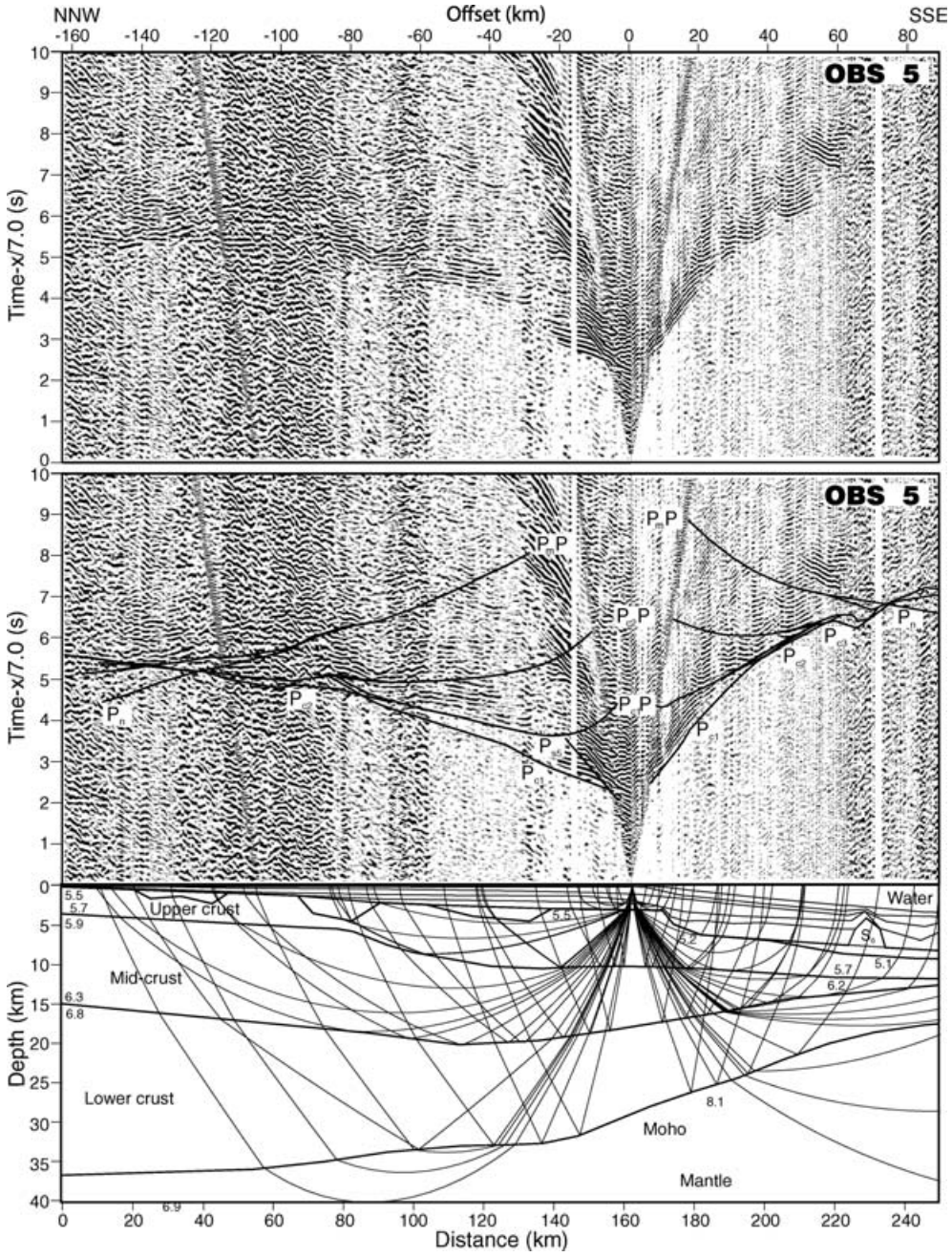

Figure A2. Record section for OBS 5 (hydrophone component). OBS 5 is located at the shelf edge. On this record section, P_{c1} and P_{c2} and their corresponding reflection phases $P_{c1}P$ and $P_{c2}P$ are observed. P_mP imaged at far offsets. P_n is less clear at offsets around −140 km.

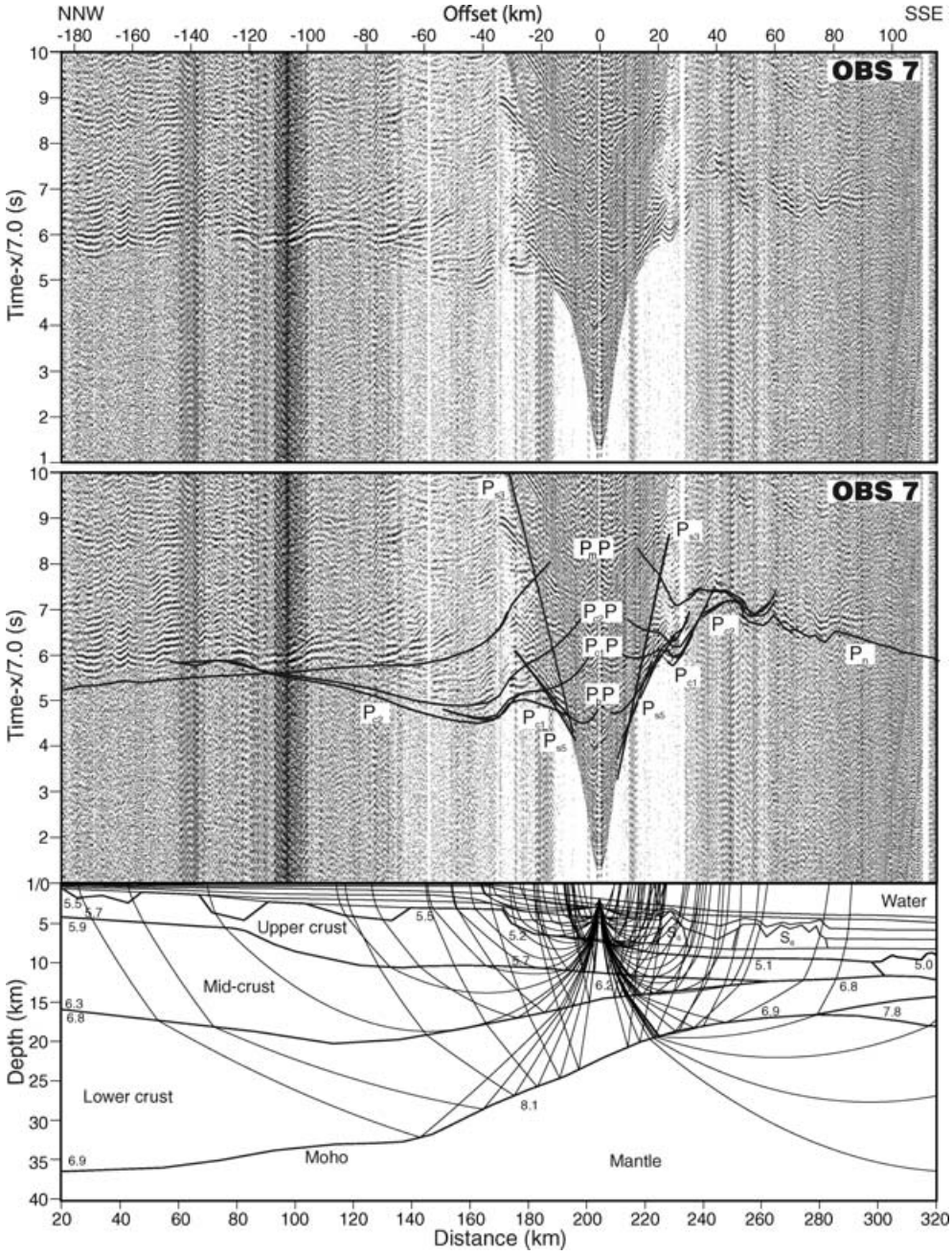

Figure A3. Record section for OBS 7 (vertical geophone component). On this OBS, P_{c1} and P_{c2} and their corresponding reflections $P_{c1}P$ and $P_{c2}P$ are observed. P_mP is imaged at offsets from −40 to −182 km. P_n is distorted by salt diapirs but is identifiable at offsets 50–100 km.

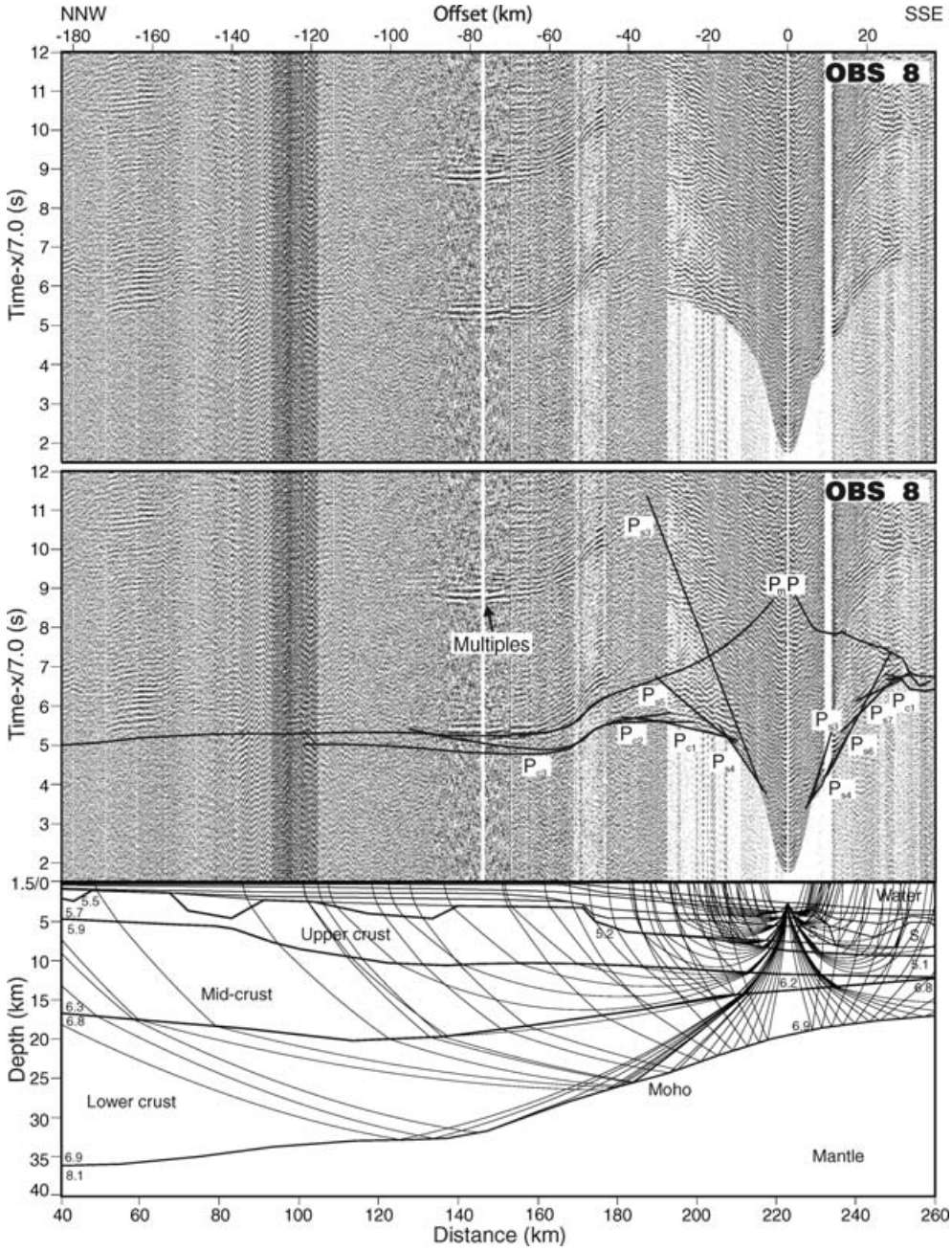

Figure A4. Record section for OBS 8 (hydrophone component). The record section shows P_{c1} and weak P_{c2} and P_{c3} phases of the crustal layers beneath the slope area where most thinning of the continental crust occurs (distance 150–250 km). P_mP and its multiple from offsets −40 to −180 km provide constraints for the Moho geometry beneath the slope area.

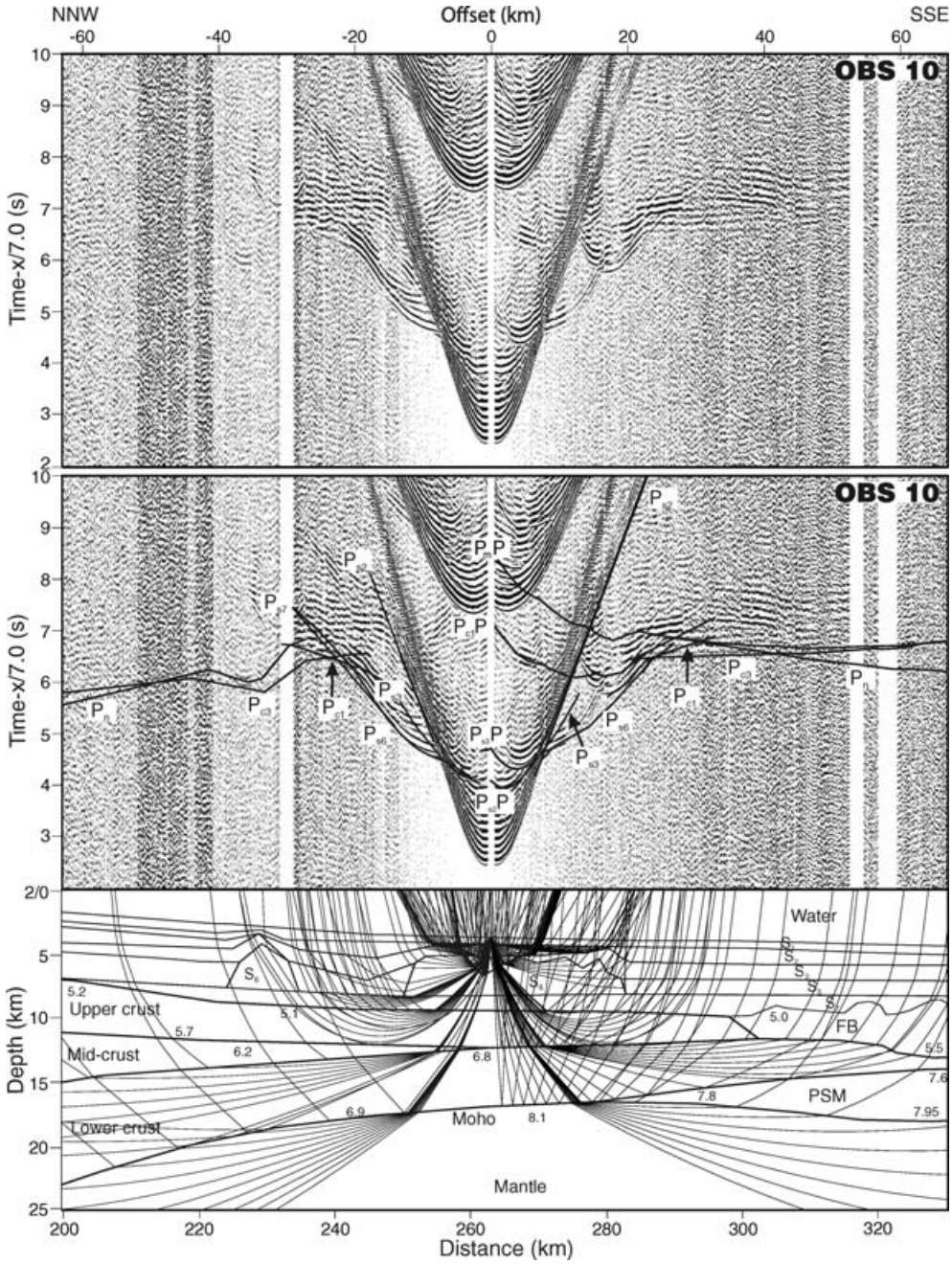

Figure A5. Record section for OBS 10 (hydrophone component). OBS 10 is located at over the salt diapir structure. Refraction from the salt units (P_{s6}) is observed. Phase P_{c1} is disturbed by the irregular geometry of the salt diapirs. Phase P_{c3} is imaged on the SSE side at offsets 20–50 km and is weak but identifiable on the NNW side from −30 to −40 km. P_mP is observed at offsets 20–60 km and P_n is observed at far offsets.

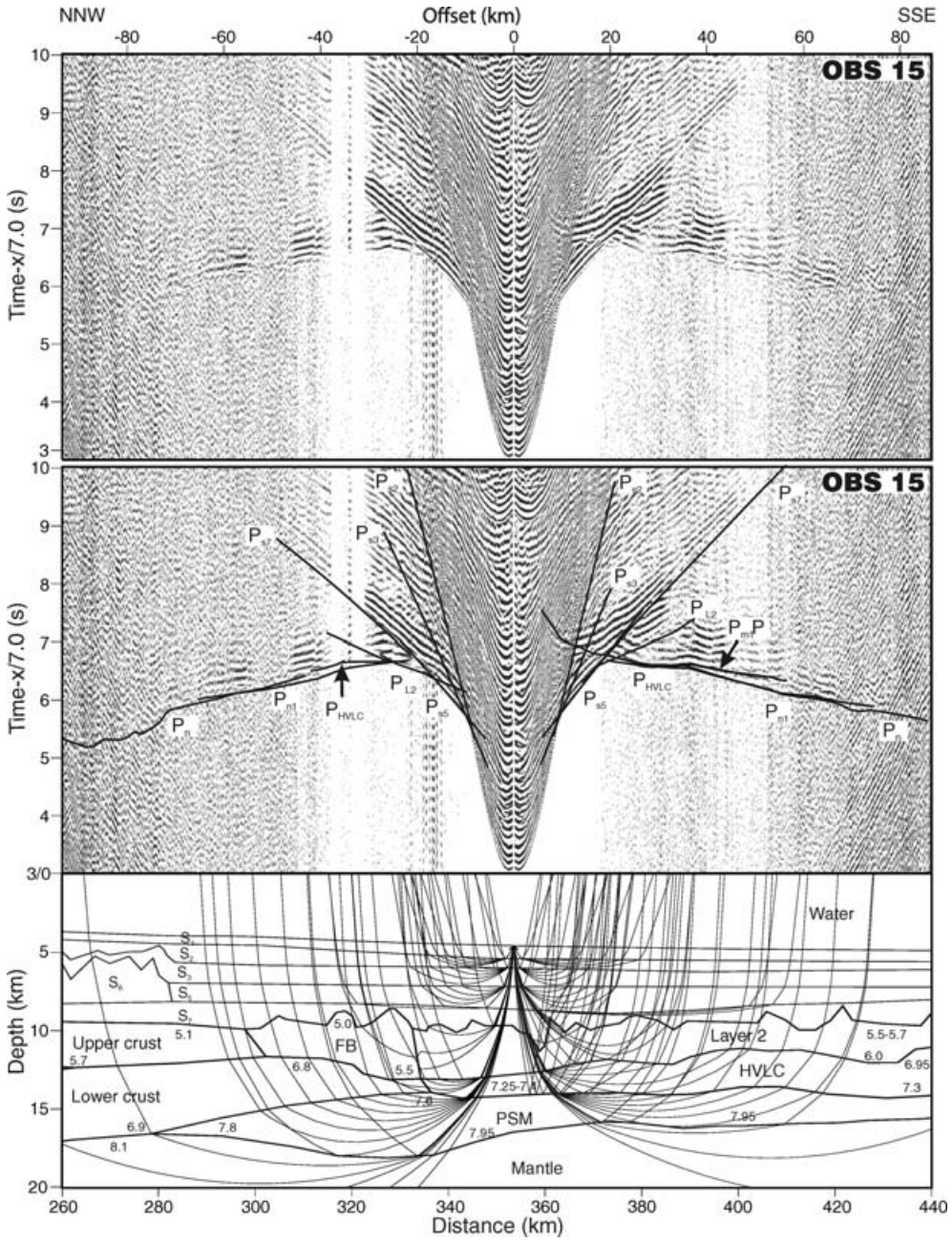

Figure A6. Record section with for OBS 15 (vertical geophone component). Phases P_{L2}, P_{HVLC}, P_{n1} and P_n are imaged on both sides as first or recognizable second arrivals. The reflection $P_{m1}P$ from the base of the HVLC layer appears at the SSE side at offsets 40–60 km.

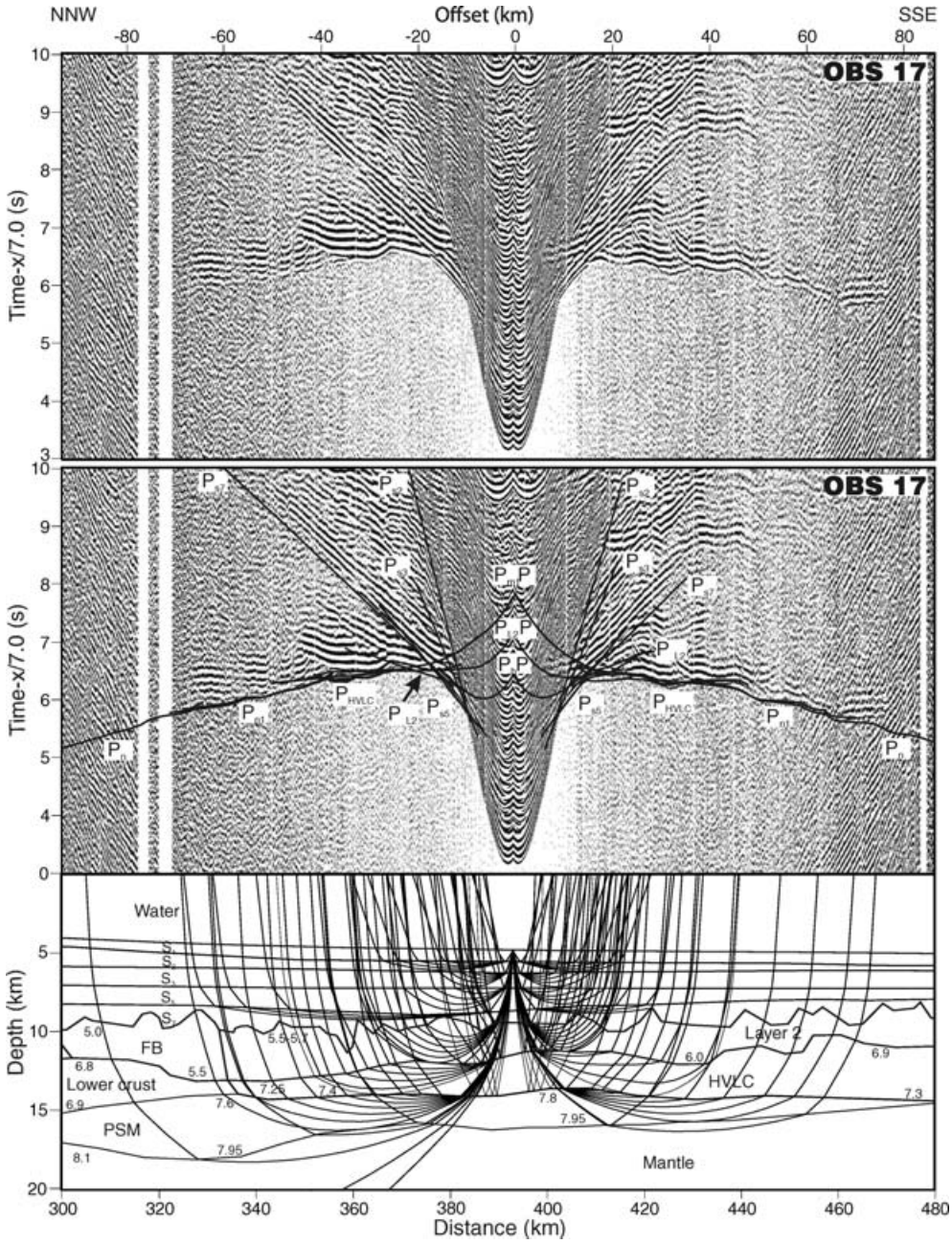

Figure A7. Record section with for OBS 17 (vertical geophone component). Phases P_{L2} and P_{HVLC} are imaged as first or recognizable second arrivals. Reflection P_{m1} P and refraction Phase P_{n1} are observed on both sides. P_n is observed at far offsets.

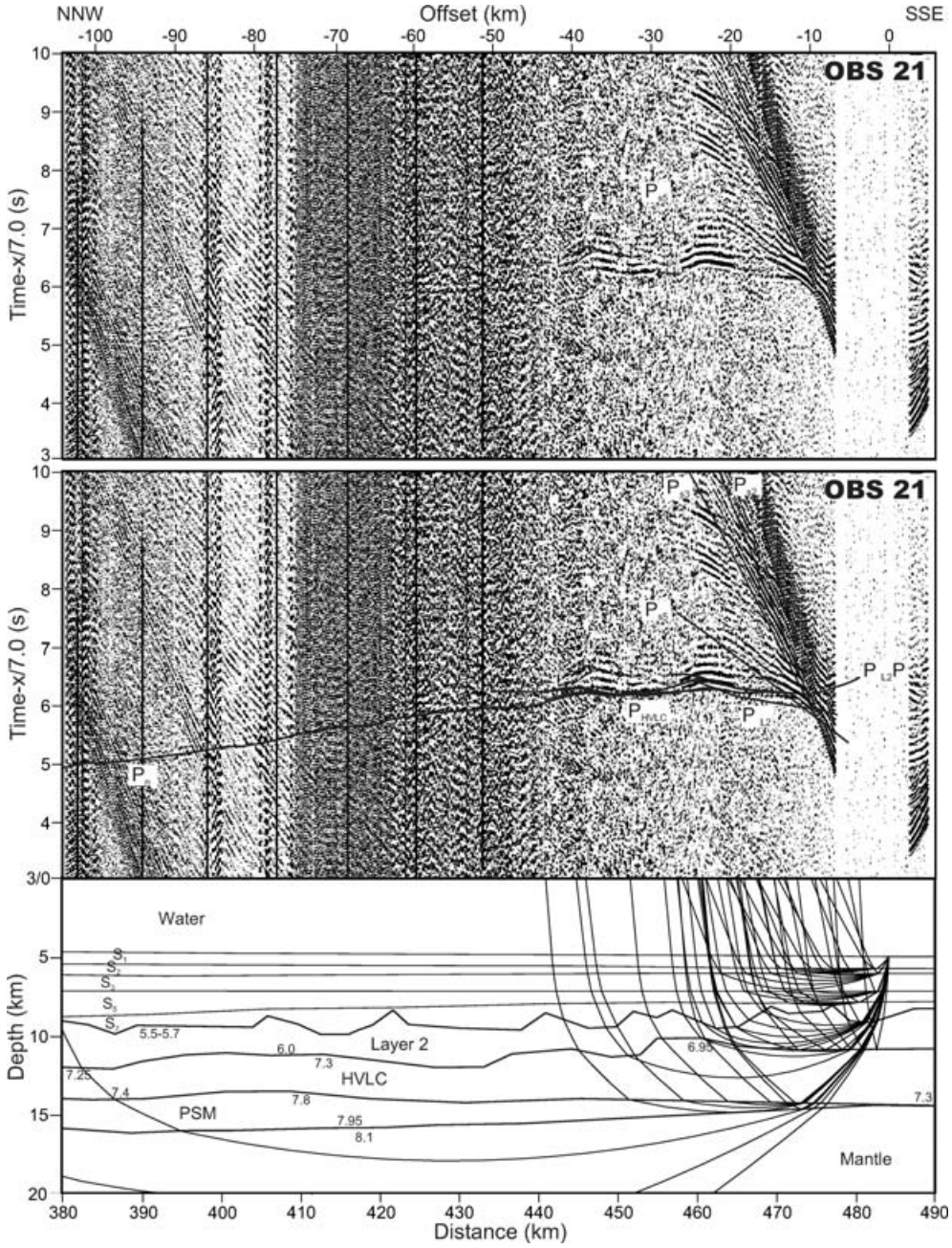

Figure A8. Record section for OBS 21 (hydrophone component). OBS 21 is located at the seaward end of the profile. Phases P_{L2} and P_{HVLC} are weakly imaged. Mantle refraction (P_n) is observed at far offsets between −75 and −100 km as recognizable arrivals.